SEDIMENTOLOGY the journal of the International Association of Sedimentologists

Sedimentology (2021) doi: 10.1111/sed.12882

Contourite depositional system after the exit of a strait: Case study from the late Miocene South Rifian Corridor, Morocco

WOUTER DE WEGER*, FRANCISCO JAVIER HERNÁNDEZ-MOLINA*, OLMO MIGUEZ-SALAS†, SANDRA DE CASTRO*, MIGUEL BRUNO‡, DOMENICO CHIARELLA*, FRANCISCO JAVIER SIERRO§, GRAHAM BLACKBOURN¶ and MOHAMED AMINE MANAR**

**Department of Earth Sciences, Royal Holloway University of London, Egham, Surrey, TW20 0EX, UK (E-mail: Wouter.DeWeger.2017@live.rhul.ac.uk)*

†Departamento de Estratigrafía y Paleontología, Universidad de Granada, Avd. Fuentenueva s/n, Granada, 18002, Spain

‡CACYTMAR, Universidad de Cádiz, Campus de Puerto Real S/N, Puerto Real, Cádiz, 11510, Spain

§Departamento de Geología, Universidad de Salamanca, Plaza de los Caídos, Salamanca, 37008, Spain

¶Blackbourn Geoconsulting, 26 East Pier Street, West Lothian, Bo'ness, EH51 9AB, UK

***Office National des Hydrocarbures et de Mines (ONHYM), 34, Avenue Al Fadila, Rabat, BP 99, Morocco*

Associate Editor – Christian Betzler

ABSTRACT

Idealized facies of bottom current deposits (contourites) have been established for fine-grained contourite drifts in modern deep-marine sedimentary environments. Their equivalent facies in the ancient record however are only scarcely recognized due to the weathered nature of most fine-grained deposits in outcrop. Facies related to the erosional elements (i.e. contourite channels) of contourite depositional systems have not yet been properly established and related deposits in outcrop appear non-existent. To better understand the sedimentary facies and facies sequences of contourites, the upper Miocene contourite depositional systems of the South Rifian Corridor (Morocco) is investigated. This contourite depositional system formed by the dense palaeo-Mediterranean Outflow Water. Foraminifera assemblages were used for age-constraints (7.51 to 7.35 Ma) and to determine the continental slope depositional domains. Nine sedimentary facies have been recognized based on lithology, grain-size, sedimentary structures and biogenic structures. These facies were subsequently grouped into five facies associations related to the main interpreted depositional processes (hemipelagic settling, contour currents and gravity flows). The vertical sedimentary facies succession records the tectonically induced, southward migration of the contourite depositional systems and the intermittent behaviour of the palaeo-Mediterranean Outflow Water, which is mainly driven by precession and millennial-scale climate variations. Tides substantially modulated the palaeo-Mediterranean Outflow Water on a sub-annual scale. This work shows exceptional examples of muddy and sandy contourite deposits in outcrop by which a facies distribution model from the proximal continental slope, the contourite channel to its adjacent contourite drift, is proposed. This model serves as a reference for contourite recognition both in modern environments and the ancient record. Furthermore, by establishing the hydrodynamics of overflow behaviour a framework is provided that improves process-based interpretation of deep-water bottom current deposits.

Keywords Bottom currents, channels, contourites, deep-water sedimentation, Late Miocene, Morocco, Rifian corridors, tides.

INTRODUCTION

Over the last decade there has been a significant increase in published evidence of deep-marine bottom current processes and associated deposits, contourites. Most of these works however are based on two-dimensional and three-dimensional seismic profiles (Faugères *et al.*, 1999; Paulat *et al.*, 2019), some from wells and cores (Gonthier *et al.*, 1984; de Castro *et al.*, 2020a,b; Hovikoski *et al.*, 2020), but there is still very little information from the exposed ancient record.

Sedimentation in deep-marine environments is predominantly controlled by pelagic, gravitational and contouritic processes, or their mixed occurrence (Fonnesu *et al.*, 2020; Shanmugam, 2020; Stow & Smillie, 2020). When bottom currents represent the dominant depositional process, a contourite depositional system (CDS) develops (Hernández-Molina *et al.*, 2008). Currently, there is no widely accepted model for such systems, but they are generally composed of a combination of depositional (related to low current velocities) and erosional (related to high current velocities) elements. Both elements result from the hydrodynamic behaviour of water masses that reach and interact with the seafloor and are conditioned by bathymetry (Hernández-Molina *et al.*, 2006).

As a result of the differentiation between areas prone to low current and high current velocities, contourite deposits are generally divided into muddy contourites (fine-grained) or sandy contourites (coarse-grained) (Stow & Faugères, 2008). Most of the evidence used to identify contourites is based on the large morphological features of depositional elements (Faugères *et al.*, 1999; Hernández-Molina *et al.*, 2008), particularly on the large depositional contourite drifts, with less attention on the possible erosional contourite elements. Accordingly, the only generally accepted contourite facies model is the bi-gradational model (Faugères *et al.*, 1984; Gonthier *et al.*, 1984; Stow & Faugères, 2008) defined for fine-grained contourite drifts. Therefore, it is often wrongly assumed that bottom currents only generate muddy contourite deposits, disregarding the fact that some authors highlighted the occurrence of sandier sediments deposited or reworked by the action of bottom currents. These sandier sediments are mainly found within contourite erosional elements, such as, channels (Hernández-Molina *et al.*, 2014a,b; Capella *et al.*, 2017a; Brackenridge *et al.*, 2018; de Weger *et al.*, 2020), contourite terraces (Viana *et al.*, 1998; Hernández-Molina *et al.*, 2009, 2016a,b, 2018; Mutti *et al.*, 2014; de Castro *et al.*, 2021) or in mixed turbidite and contourite depositional systems (Rebesco *et al.*, 2002; Creaser *et al.*, 2017; Sansom, 2018; Fonnesu *et al.*, 2020; Fuhrmann *et al.*, 2020; Rodrigues *et al.*, 2021).

The natural evolution of a CDS comprises the lateral migration of both depositional and erosional elements. This implies that, for example, drifts develop on top of channels (Chen *et al.*, 2020) or channels erode into drifts (Llave *et al.*, 2001; Hernández-Molina *et al.*, 2008, 2014b; Chen *et al.*, 2020). This migration has been identified using seismic data, but the sedimentary facies and facies sequences related to these migrating environments are currently not established. This is a partial consequence of the lack of recognized CDS in outcrop which show lateral and vertical facies variability.

Contourite outcrops, as mentioned earlier, have however only been scarcely recognized. This likely results from the lack of distinct diagnostic contourite features, hindering the scientific community to identify these deposits in outcrop (Hüneke & Stow, 2008; Rebesco *et al.*, 2014; Shanmugam, 2017). Furthermore, the problematic identification of muddy contourites in outcrop, for which most diagnostic criteria (the bi-gradational model and morphological features) exists, results from their relatively homogeneous and severely bioturbated nature (Gonthier *et al.*, 1984), but also because most fine-grained outcrops are usually severely weathered. The recognition of sandy contourites, for which no true diagnostic criteria exist, is mainly hindered by the process-based interpretation of deep-marine sediments. There is a general idea that sandy deposits only enter the deep-marine realm by gravitational processes, and it is regularly wrongly assumed that deep-marine bottom currents are only related to thermohaline circulation, not reaching current velocities capable of reworking, transporting and

depositing sandy sediment. The poorly understood hydrodynamic properties of deep-marine water masses that reach and interact with the seafloor stand in the way of such process-based interpretation of bottom current deposits.

This paper investigates the sedimentary record of a well-exposed late Miocene CDS in the Saiss Basin, associated with the South Rifian Corridor of Morocco (Fig. 1). The main objectives of this study are to: (i) determine the geometries, sedimentary facies and facies sequences related to the lateral migration of the CDS; (ii) interpret its evolution; (iii) investigate the dynamics of overflow behaviour in a confined basin; and (iv) provide the much-needed clarification on the role of bottom currents to improve process-based interpretation for deep-marine contourites. The results presented herein will thus also serve as a reference for the recognition of contourite deposits.

STUDY AREA AND GEOLOGICAL SETTING

The studied sections are exposed in the Saiss Basin in northern Morocco (Fig. 1). This basin is part of the external zone of the Rif-Betic Arc, or Gibraltar Arc which forms an arc-shaped orogenic belt surrounding the Alboran Sea in the westernmost Mediterranean region.

The Betic and Rifian corridors were late Miocene marine gateways that allowed Mediterranean–Atlantic water exchange (Fig. 1). The Rifian corridors evolved during the latest stage of Africa–Iberia collision in the late Tortonian (*ca* 8 Ma) as south-westward migrating foreland basins (Feinberg, 1986; Wernli, 1988; Sani *et al.*, 2007). These foreland basins were limited northward by the earlier exhumed Rif orogenic wedge (Iribarren *et al.*, 2009) and southward by the Atlas Mountains (Barbero *et al.*, 2011). The corridor is generally divided into two strands (Fig. 1A); the North Rifian Corridor (NRC) related to the Rifian Intramontane basins, and the South Rifian Corridor (SRC) related to the Taza-Guercif and Saiss basins (Wernli, 1988). Both strands were separated by the chaotic complex of the accretionary wedge (Fig. 2), the emplacement of which over the African foreland started during the early Tortonian (Feinberg, 1986; Flinch, 1993; Chalouan & Michard, 2004; Michard *et al.*, 2008). Since the accretionary wedge is locally overlain by Upper Miocene marine sediments, the Rifian corridors were at times a single wide gateway westward of the Taza Strait (Fig. 1). The central portion of the Taza Strait was characterized by a sill (the Taza Sill) (Flecker *et al.*, 2015; Capella *et al.*, 2017a; de Weger *et al.*, 2020), which formed a submerged topographic high related to the east–west oriented thrust-front overlying the north-east/south-west oriented Middle Atlas. The Taza Strait separated the Taza–Guercif and the Saiss basins and the Taza Sill controlled the water mass exchange between the Mediterranean and the Atlantic during the late Miocene (Capella *et al.*, 2017a; de Weger *et al.*, 2020). The westernmost part of the Rifian corridors was in the Gharb Basin where both the Rifian Intramontane and Saiss basins merged (Sani *et al.*, 2007). The Gharb Basin was located just west of the Prerifian Ridges (Figs 1A and 2) which form the arcuate shaped southernmost leading edge of the Rif Chain.

The development of the Prerifian Ridges mainly took place during two phases (Roldán *et al.*, 2014). The initial development occurred during the middle to late Miocene, accompanied by the south-westward gravitational emplacement of the accretionary wedge (Capella *et al.*, 2017b). The second phase of compressional deformation happened during the late Tortonian to early Messinian during which the Prerifian Ridges were formed. These ridges represented a tectonically uplifting, likely subaqueous relief on the northern margin of the South Rifian Corridor during the Tortonian (Roldán *et al.*, 2014; de Weger *et al.*, 2020).

Lithostratigraphy of the Saiss Basin

The middle Miocene–late Pliocene Saiss Basin fill stratigraphy (Fig. 3) overlies a major angular unconformity. The basal foredeep sediments are mainly divided into two formations: (i) the Benni Ammar White Marl Formation, which pre-dates the emplacement of the accretionary wedge (Fig. 3); and (ii) the Blue Marl Formation, mainly post-dating its emplacement. Within the Blue Marl Formation up to 120 m thick sands were locally deposited (Capella *et al.*, 2017a; de Weger *et al.*, 2020). The accretionary wedge, consisting of Triassic to late Miocene tectono-stratigraphic units, developed in the study area during the late Tortonian to Messinian (Sani *et al.*, 2007) coinciding with the onset of Rifian Corridor sedimentation that started around 8 Ma (Wernli, 1988; Krijgsman *et al.*, 1999; Gelati *et al.*, 2000; Hilgen *et al.*, 2000; Barhoun & Taoufio, 2008; Achalhi *et al.*, 2016). On top of the Tortonian Blue Marls, mainly limited to the south Saiss Basin but also locally along the

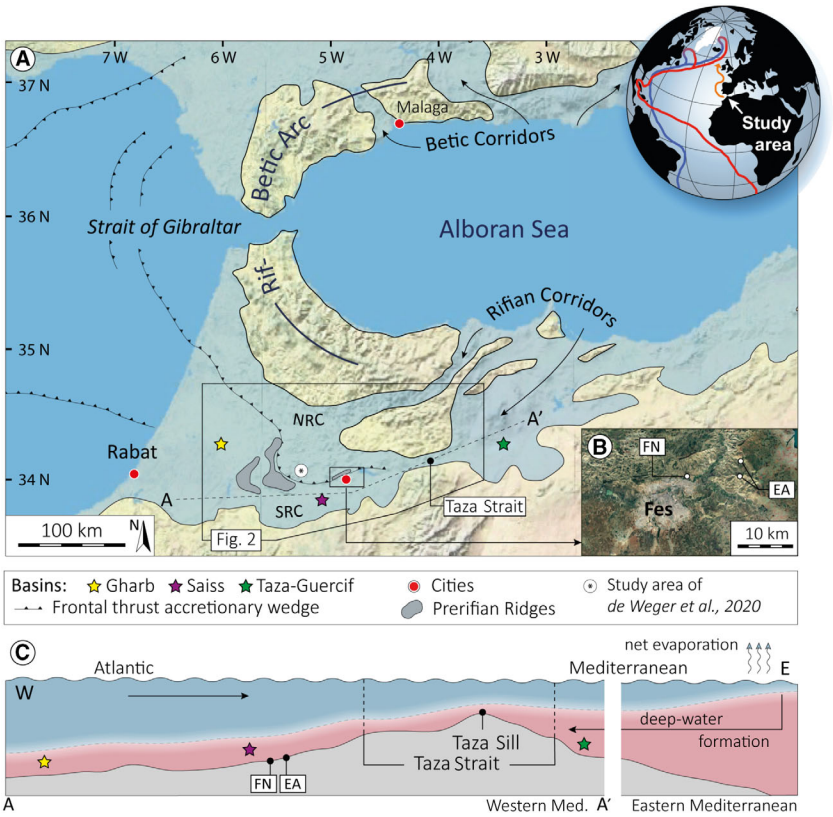

Fig. 1. (A) Satellite terrain image of the westernmost Mediterranean region, southern Spain and north-west Africa. The globe on the right-hand corner shows the location of the study area and depicts the thermohaline circulation pattern (red – shallow; blue – deep), the orange arrow indicates the pathway of the Mediterranean Outflow Water (MOW). In transparent blue a late Miocene palaeogeographic overlay of the Betic and Rifian corridors, NRC = North Rifian Corridor and SRC = South Rifian Corridor, after de Weger *et al.* (2020). The location of the main geological features, such as the Gharb, Saiss and Taza–Guercif basins, the Prerifian Ridges and the Taza Strait are indicated. (B) Satellite image showing the location of the study areas. The abbreviations stand for the section names; FN = Fes-north and EA = El Adergha. (C) Late Miocene reconstruction through the SRC, cross-section A–A', of which the location is indicated in (A). The SRC accommodated Atlantic–Mediterranean exchange of surficial Atlantic and Mediterranean Deep Water.

northern margin of the Saiss basin, early Messinian to middle Pliocene shelfal and nearshore marine marls and sandstones are deposited (Capella *et al.*, 2018). These shallow-marine deposits are in turn locally truncated by an erosional unconformity and overlain by lacustrine limestones (Taltasse, 1953; Capella *et al.*, 2018).

PALAEOCEANOGRAPHIC SETTING

During the late Miocene, an Atlantic – Mediterranean connection existed through the Betic Corridor in southern Spain and the Rifian corridors in northern Morocco (Fig. 1A). After subduction of the accretionary wedge, as well as of the external Betic and Rif fold–thrust belts largely came to a halt in the late Tortonian (van Hinsbergen *et al.*, 2014), tectonic uplift first took over in the Betic at *ca* 7.8 Ma (Betzler *et al.*, 2006; Krijgsman *et al.*, 2006) and slightly later, by *ca* 7 Ma, in the Rif orogeny (Capella *et al.*, 2017b; Tulbure *et al.*, 2017). All the Betic – Atlantic – Mediterranean connections were closed due to Africa–Iberia convergence by the early Messinian (Spakman *et al.*, 2018). By *ca* 7.2 Ma the North Rifian Corridor was closed (Tulbure *et al.*, 2017) but the South Rifian Corridor was still open during the earliest Messinian recording a transition to continental and lacustrine deposits by *ca* 6.9 Ma (Capella *et al.*, 2017a). Since there is no evidence of a

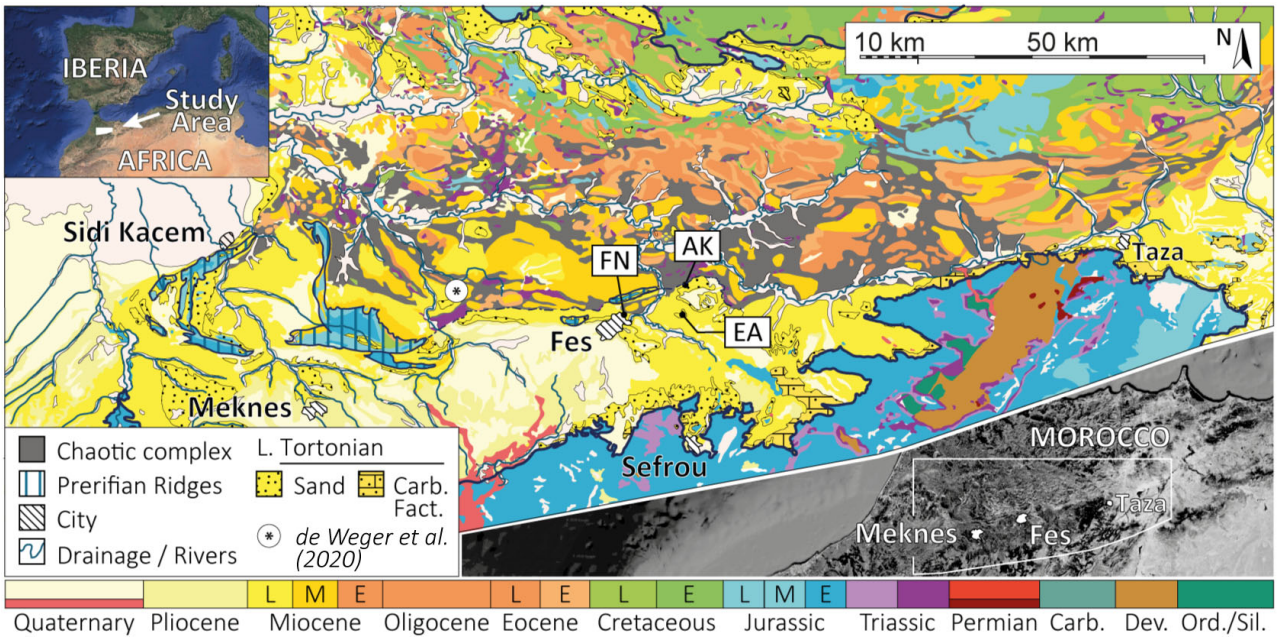

Fig. 2. Regional geological map of the study area including the locations of the studied Upper Miocene outcrops; El Adergha (EA), Fes-north (FN) and Ain Kansera (EA) (modified after Saadi *et al.*, 1980). Carb. Fact = carbonate factory, L = late, M = middle and E = early. Satellite images are derived from Google Earth©.

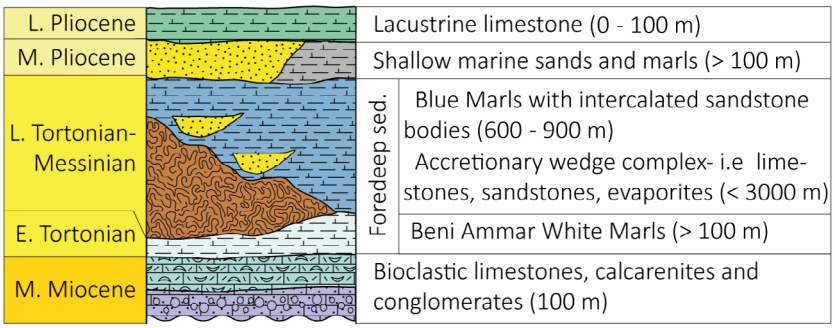

Fig. 3. Middle Miocene to late Pliocene lithostratigraphy of the Saiss Basin. The intercalated sandstone bodies in the late Tortonian to Messinian Blue Marl Formation belong to the sections studied herein.

Mediterranean–Atlantic gateway through the Betic and Rifian corridors during the Messinian, the Gibraltar Corridor arguably became the sole Atlantic gateway during this period (Krijgsman *et al.*, 2018). Between *ca* 5.97 Ma, the time of the onset of the Mediterranean Salinity Crisis (Hsü *et al.*, 1973; Ryan & Hsü, 1973), and *ca* 5.6 Ma, the Gibraltar Corridor accommodated a two-way connection (Simon & Meijer, 2017) after which it only facilitated Mediterranean inflow until *ca* 5.33 Ma (Krijgsman *et al.*, 2018).

After the closure of all but one of the Betic corridors in the late Miocene, the North Rifian Corridor maintained the inflow of Atlantic water in the Mediterranean (Tulbure *et al.*, 2017) whereas the South Rifian Corridor maintained Atlantic–Mediterranean water exchange similar to what is currently occurring in the Strait of Gibraltar (de Weger *et al.*, 2020). The South Rifian Corridor likely accommodated inflow of the North Atlantic Surficial Water (NASW) and the Eastern North Atlantic Central Water (ENACW) into the Mediterranean, overriding a warm and highly saline water mass associated with the palaeo-Mediterranean Outflow Water (MOW). The water mass of the palaeo-MOW was formed due to net evaporation and cooling in the eastern Mediterranean (Fig. 1B). This net evaporation and cooling increased the density of Mediterranean surface water (Straume *et al.*,

2020) which was 'continuously' replenished by cold and less saline Atlantic water. Subsequently, this increase in density forced this water to sink and ventilate the water column, a process known as intermediate and deep-water formation (Millot, 1999; Candela, 2001). The formation of Mediterranean Deep Water (MDW) (and thus the formation of water masses related to the palaeo-MOW) resulted in a significant density gradient, or water mass stratification, between the Mediterranean and the Atlantic. This density gradient drove water mass exchange by two-way flow (Rohling *et al.*, 2015; Simon *et al.*, 2017). During the late Miocene a dense palaeo-MOW flowed over the Taza Sill through the Taza Strait (Fig. 1) downward into and through the South Rifian Corridor towards the Atlantic (de Weger *et al.*, 2020).

METHODOLOGY

Two well-exposed late Miocene outcrops, El Adergha and Fes-north (Figs 1, 2, 4A and 4B), from the South Rifian Corridor are described in detail in this paper to unravel the facies successions and their vertical and lateral changes. The El Adergha section has previously partly been described by Capella *et al.* (2017a) and their results have been taken into consideration. The El Adergha section has been however re-interpreted and has been put into a new palaeogeographic framework based on the results of this study. A third section, Ain Kansera (Fig. 2), previously studied by Capella *et al.* (2017a), has also been reviewed and considered for discussion. Because present observations and interpretations do not significantly divert from those made previously, the Ain Kansera section is not described in detail in this work.

The sedimentary successions were studied by standard field techniques which include bed-scale characterization of sedimentological and stratigraphic elements. Two stratigraphic sections were measured at centimetre to metre-scale to document the key features such as lithology, grain-size and sorting, sedimentary structures, bedding thickness, nature of bed contacts and palaeocurrent indicators. These features form the basis for the facies analysis. Sixty-four palaeoflow indicators (cross-stratification, ripple lamination and sole marks) were recorded across both outcrops.

A bed-by-bed ichnological analysis was conducted. The distribution, types and abundance of trace fossils were characterized to describe stratigraphic trends throughout the sections. Ichnological observations focused on orientation, shape, length and diameter of individual burrow segments, configuration of burrow systems and taphonomy, allowing for ichnotaxonomical assignation.

Seven samples for petrographic analysis (Table S1; Figs S1 and S2) were derived from indurated sand beds. Two sets of thin sections were prepared for each sample, one of which was impregnated with dyed resin to highlight porosity. The samples were examined under a Nikon Optiphot-pol petrographic microscope (Nikon, Tokyo, Japan) with integral Canon EOS-50D camera system (Canon Inc., Tokyo, Japan). Modal analysis was carried out on three samples (EA3, FN1 and EA5) by determining the composition at 300 points using a stepping stage and associated PETROG™ software (Table S1).

Eight samples for biostratigraphy, derived from marls that were more than 50 cm below the rock's exposed surface, were analyzed. Three samples for the El Adergha section were compared to what has been published by Capella *et al.* (2017a) to integrate their results. Five new samples from the Fes-north section were compared to the biostratigraphic framework published in Capella *et al.* (2017a) and Tulbure *et al.* (2017) to date these samples based on quantitative changes in abundance of keeled and unkeeled *Globorotalids*.

The palaeowater-depth was inferred from the benthic foraminifera assemblages of the biostratigraphic samples. The specific assemblages and relative abundance of benthic species were associated with depth ranges identified in the existing literature (Pérez-Asensio *et al.*, 2012). The mixed occurrence of shallow-water and deep-water species is considered the result of downslope transport and, hence, the deeper-water species are deemed most reliable in depositional depth estimates.

RESULTS

Studied sections

The sections, El Adergha and Fes-north, comprise sandstone-rich intervals intercalated within the Blue Marl Formation (Figs 4 and 5). The sections are located 9.6 km apart (Figs 2 and 5). The El Adergha outcrop (34.076402−4.860522) is located on the northern flank of the Saiss Basin

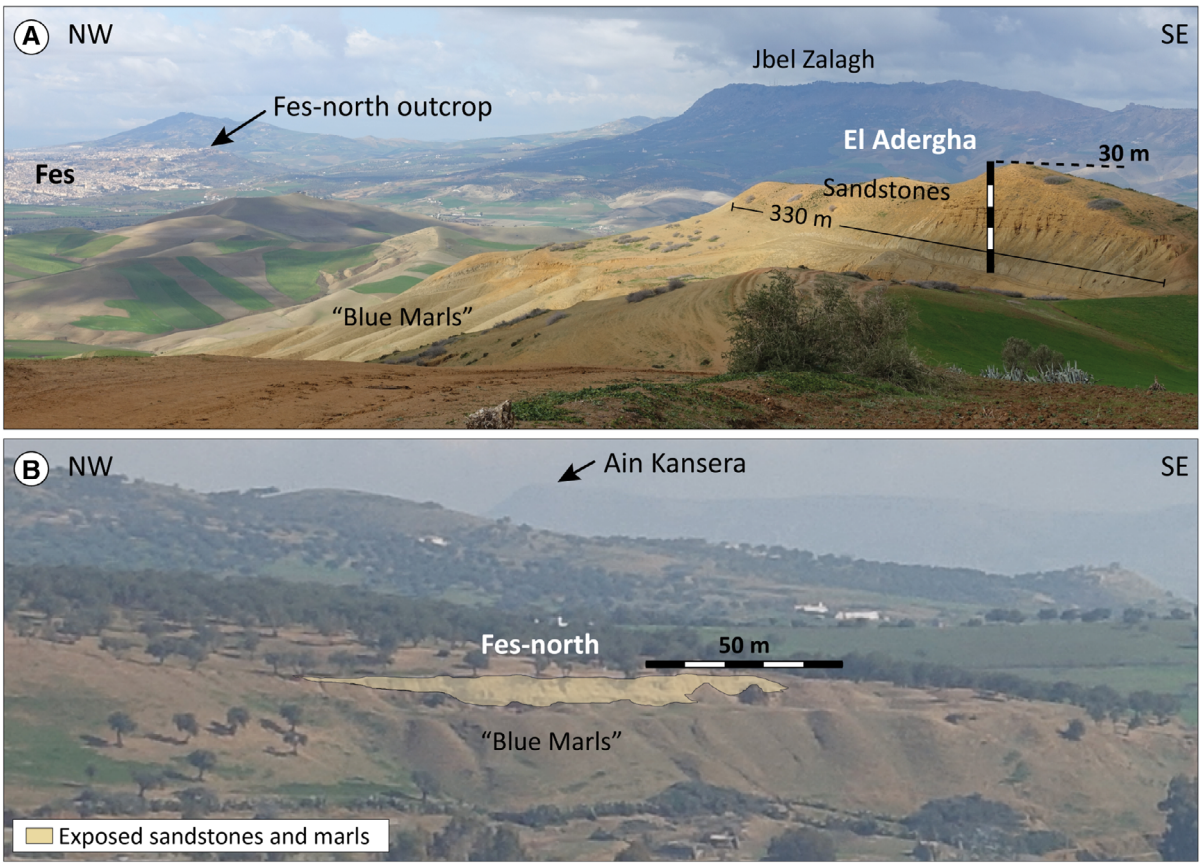

Fig. 4. Panoramic view of the El Adergha (A) and Fes-north (B) outcrops. These pictures highlight the general exposed geometries and the scale of the outcrops. Due to the location of the Fes-north section being far away from the nearest vantage point no better pictures are currently available.

(Figs 1 and 2B), 10 km ENE of the city of Fes and 7.5 km south-east of the westernmost expression of the Prerifian Ridges Jbel Zalagh. The section forms a topographic high with an up to 15 m thick sandstone body at its peak (Fig. 4A). Below the sandstone an up to 1000 m thick fine-grained succession related to the Blue Marl Formation occurs. The south-western flank is steeply inclined to near vertical whereas the north-eastern flank shows a much shallower inclination. The upper sandy part of the outcrop forms a gently sloping concave geometry which measures roughly 330 m (west–east) by 100 m (north–south) in a horizontal plane (Fig. 4A).

The Fes-north section (34.076337−4.964840) is located north of the city of Fes, 3 km south of Jbel Zalagh and *ca* 7 km west of the El Adergha section (Figs 2B and 4B). The Fes-north section forms a north-east/south-west striking topographic sandy ridge that is well-exposed for roughly 100 m horizontally and 7 m vertically (Fig. 4B). The present-day shape of this outcrop is due to the soil and vegetation cover and does not represent the primary lithosome profile of the outcrop in cross-sectional view. The sandstone ridge overlies a succession of marlstone pertaining to the Blue Marl Formation.

Age and depositional domain

The studied outcrops show a range of facies related to different depositional environments, as such, the age and depositional domain estimates will be treated individually for each section. The biostratigraphic results from the El Adergha section indicate a depositional period between 7.51 Ma and 7.25 Ma for the uppermost 100 m of the section (Fig. 5). The sand-rich interval at the top, consisting of the uppermost 28 m (Figs 5 and 6) has been dated between 7.35 Ma and 7.25 Ma based on the common occurrence of *Globorotalia menardii* 5. This

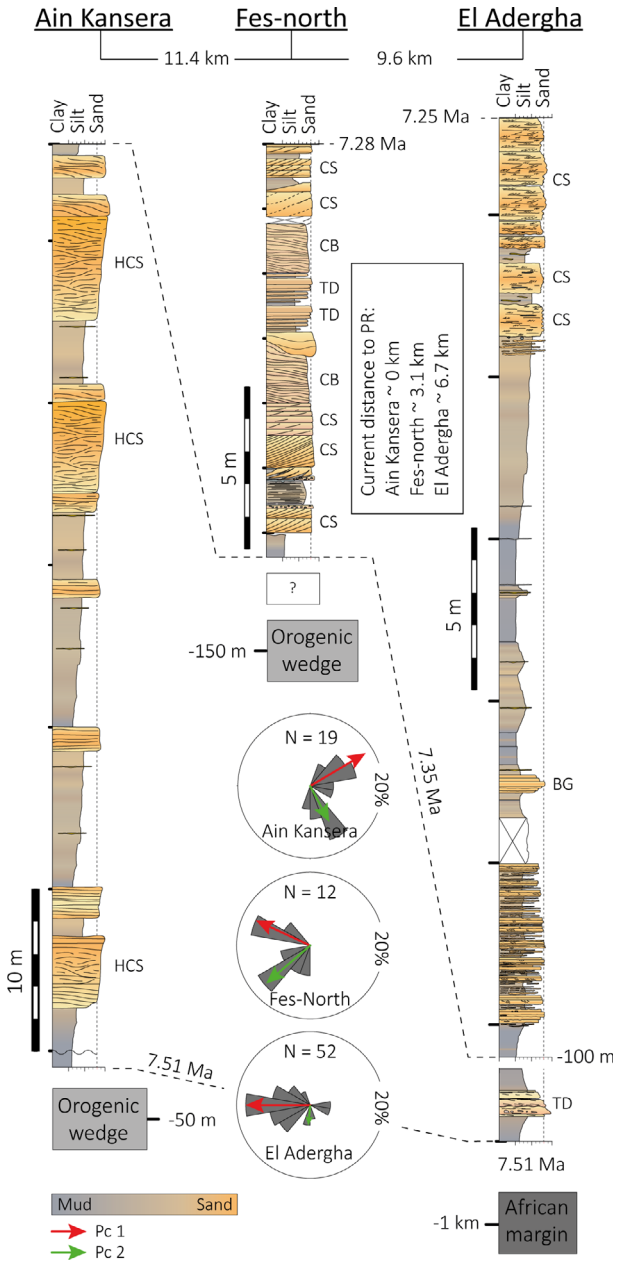

Fig. 5. Sedimentary logs for the Ain Kansera (modified after Capella *et al.*, 2017a), Fes-north and El Adergha sections. Their location is provided in Fig. 2, and their relative distance, and distance to the Prerifian Ridges is indicated. Palaeocurrents are divided in two major components, along-slope Pc 1 (red) and down-slope Pc 2 (green). The main sedimentary features are indicated next to the log. HCS = hummocky cross-stratification, CS = cross-stratification, BG = bi-gradational and TD = turbidite (see text for interpretation).

species appears frequently between its first common occurrence at 7.35 Ma and the replacement of *Globorotalia menardii* by *Globorotalia miotumida* at 7.25 Ma (Sierro, 1985; Sierro *et al.*, 1993, 2001; Hilgen *et al.*, 2000; Capella *et al.*, 2017a). Benthic foraminifer assemblages indicate a depositional domain in the slope for the blue marl package (250 to 400 m water depth) and an upper slope depositional domain (300 to 140 m water depth) for the sand package. These results are supported by the findings of Capella *et al.* (2017a).

Most of the collected samples in the Fes-north section contain abundant planktonic foraminifera. In general, keeled globorotalid forms are scarce, but *Globorotalia menardii* 5 is common in some samples and *Globorotalia menardii* 4 is usually rarer. Based on this, this section is dated as being between the last common occurrence of *Globorotalia menardii* 4 at 7.51 Ma and the replacement of *Globorotalia menardii* by *Globorotalia miotumida* at 7.25 Ma (Sierro, 1985; Sierro *et al.*, 1993, 2001; Hilgen *et al.*, 2000; Capella *et al.*, 2017a; Tulbure *et al.*, 2017). The continuous presence of dominant sinistral specimen of *Globorotalia scitula*, including *Globorotalia suterae* led to a determination of an age older than 7.28 Ma, which is the age at which coiling in this group changed from sinistral to dextral (Sierro *et al.*, 1993). The benthic foraminifer assemblages indicate a depositional domain in the slope with abundant deeper water taxa such as *Lagena*, *Syphonina*, *Gyroidina*, *Melonis*, etc., mixed with shallow water benthic species such as *Elphidium*, *Ammonia*, *Nonion*, *Lobatula*, etc. The percentage of planktonic foraminifera relative to benthic foraminifera is on average higher than 60%. Some samples contain reworked specimens from the Eocene to middle Miocene.

Palaeogeographic reconstruction based on obtained ages and depositional domains

de Weger *et al.* (2020) recently described a contourite channel system and the intermittent behaviour of palaeo-Mediterranean Outflow Water (palaeo-MOW). The system described therein is located north of the Prerifian Ridges, compared to the outcrops described here (Figs 1 and 2). Furthermore, the deposits on which their interpretation is based are dated between 7.8 Ma and 7.51 Ma and are thus older than the deposits described in this study (7.51 to 7.25 Ma). Although attributed to a different stratigraphic interval, they are thought to have likely been formed by similar deep-marine processes controlled by the overflow of the late Miocene palaeo-MOW.

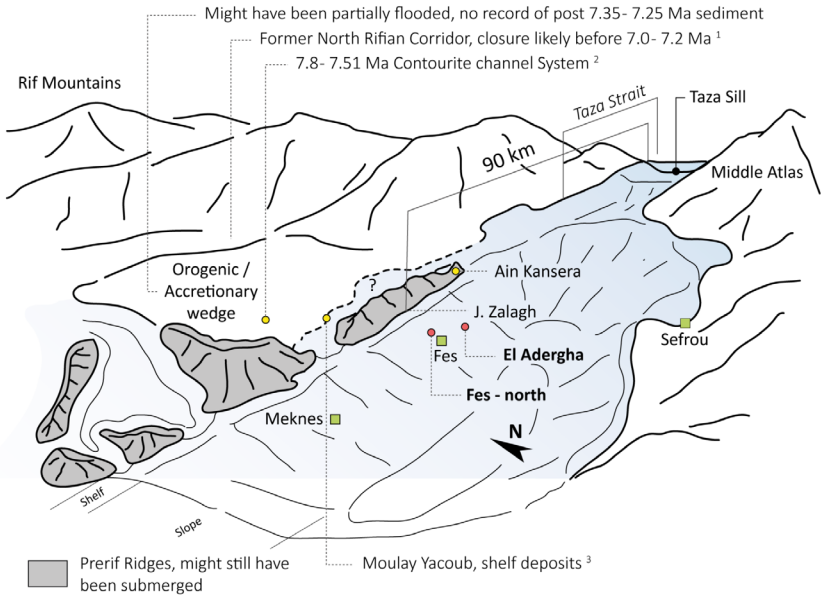

Fig. 6. Palaeogeographic reconstruction of the late Miocene South Rifian Corridor (7.51 to 7.25 Ma). The Prerifian Ridges (grey) might still have been submerged at this time. Red dots indicate sections studied herein. Yellow dots indicate sections previously studied, publications of these sections studied previously are denoted by superscript numbers ([1]Tulbure *et al.*, 2017, [2]de Weger *et al.*, 2020, [3]Capella *et al.*, 2018). Green squares indicate the relative location of major cities in the area.

The geographical offset between the contourite depositional system north of the Prerifian Ridges (de Weger *et al.*, 2020) and the El Adergha and Fes-north sections (Figs 1 and 2) has been related to the tectonic emplacement of these ridges. As described by Roldán *et al.* (2014), the Prerifian Ridges evolved since the late Miocene to the present. The northern channels were located on the frontal part of the accretionary wedge and recorded sedimentation until 7.51 Ma; however, once the Prerifian Ridges became more prominent during the late Tortonian, around 7.51 Ma, the main palaeo-MOW pathway was forced south of these ridges (Fig. 5), abandoning the northern channels. Further evidence for these changes is found in the Ain Kansera section described by Capella *et al.* (2017a). The Ain Kansera section, dated between 7.51 Ma and 7.35 Ma, consists of shallow-marine infralittoral deposits, and is located near the easternmost physical expression of the Prerifian Ridges, closer compared to the El Adergha and Fes-north sections (Fig. 5). The Ain Kansera section has previously been interpreted as a north-eastward prograding linear clastic coast with depositional water-depths ranging between 15 m and 100 m (Capella *et al.*, 2017a).

Based on the palaeogeographic reconstruction performed by Capella *et al.* (2017a), the thickness of underlying deposits for each section to the nearest expression of the orogenic/accretionary wedge and the African margin (Fig. 5), and the depositional domain obtained from benthic foraminifer assemblages, the Prerifian Ridges most likely formed a north–south oriented slope on the northern margin of the South Rifian Corridor (Fig. 6). The southern boundary of the South Rifian Corridor was located near the city of Sefrou (Capella *et al.*, 2018), roughly 30 km south of the Ain Kansera section, indicating that between 7.51 Ma and 7.25 Ma the corridor was approximately 30 km wide. The Taza Sill was located 90 km eastward of the studied sections and the westernmost expression of the Prerifian Ridges is located roughly 85 km towards the west. This implies that the steeply flanked South Rifian corridor measured roughly 30 km in width and 175 km in length, westward of Taza Strait (Fig. 6).

Sedimentary facies

Nine different sedimentary facies (F1 to F9) and associated trace fossils have been distinguished in the two studied sections (Table 1; Figs 7 to 9). The sedimentary facies include: (i) F1 – fossil-rich blue marlstone; (ii) F2 – sandy marlstone; (iii) F3 – bi-gradational sandstone; (iv) F4 – heterolithic mudstone and sandstone; (v) F5 – heterolithic, cross-stratified and rippled sandstone; (vi) F6 – cross-stratified sandstone; (vii) F7 – sigmoidal, mud-draped sandstone; (viii) F8 – amalgamated, normal graded mudstone and sandstone; and (ix) F9 – deformed, heterolithic mudstone and sandstone.

Table 1. Sedimentary facies table (F1 to F9) showing the main sedimentological and ichnological characteristics and features of the studied deposits in the El Adergha (EA) and Fes-north (FN) outcrops.

Facies	Lithology	Grading	Thickness	Sedimentary structures	Accessories	Ichnology
F1 Fossil-rich blue marlstone	Fossil-rich marlstone occasionally enriched in silt to very fine-grained sand	None or subtle normal and inverse grading	Cm-scale to 100s of m-scale	Structureless with occasional laminae of up to very fine-grained sand and shell debris	–	Scarce discrete trace fossils
F2 Sandy marlstone	Fossil-rich sandy marlstone to marly, fine-grained sandstone	None, normal and inverse grading, or normal grading with sharp basal surface	Dm-scale to 10s of m-scale	Structureless, occasional bioclast enriched traction carpets and remnants of starved, fine-grained sandy ripples	–	Abundant undifferentiated trace fossil and scarce *Planolites*-like and *Thalassinoides*-like
F3 Bi-gradational sandstone	Up to medium-grained mixed compositional sand	Successive inverse and normal grading	Up to dm-scale	Planar parallel laminated to fully mottled	–	EA: scarce discrete trace fossils to abundant *Macaronichnus* and rare *Planolites*, *Thalassinoides* and *Rosselia* FN: low to moderate undifferentiated bioturbation and scarce *Planolites*
F4 Heterolithic, thin-bedded mudstone and sandstone	Heterolithic mudstone and mixed compositional up to medium-grained sandstone	Normal grading with graded or sharp basal surfaces	1 to 15 cm	Wavy, lenticular, or discontinuous planar parallel sand laminae. Ripple laminae and mud flasers. Laminated silty/sandy claystone	Numerous detrital pellets of dark, glauconite and large planktonic foraminifera	Abundant discrete trace fossils; abundant *Macaronichnus* and *Parahaentzschelinia* and rare *Planolites* and *Rosselia*

Table 1. (continued)

Facies	Lithology	Grading	Thickness	Sedimentary structures	Accessories	Ichnology
F5 Heterolithic, cross-stratified mudstone and sandstone	Heterolithic mudstone and mixed compositional, moderately-sorted to well-sorted, up to coarse-grained sandstone	Normal graded with sharp basal surfaces and occasionally mud-draped foreset boundaries	2 to 20 cm	Undulatory and tabular cross-stratified and rippled beds with occasional small (cm-scale) basal scours	Bed boundaries and sedimentary structures regularly encrusted with Fe and Mn	EA: abundant, increase of vertical burrows; abundant *Parahaentzschelinia* and *Macaronichnus*, rare *Planolites* and *Thalassinoides*. FN: vertical traces that are *Ophiomorpha*-like and *Skolithos*-like
F6 Cross-stratified sandstone	Mixed compositional up to medium-grained sandstone	None to normal grading	10 to 60 cm	Tabular, cross-stratified beds	High proportion of bioclasts and carbonate lithoclasts, muddy rip-up clasts are common	Moderate discrete trace fossils; abundant *Ophiomorpha*, occasional *Skolithos* and rare *Planolites*, *Rosselia*-like and *Thalassinoides*
F7 Sigmoidal, mud draped sandstone	Up to granule grade mixed compositional sand 'draped' by fluid muddy marls	Normal grading	Up to 30 cm	Sigmoidal, mud-draped sandstone bundles	Bed boundaries and burrow linings regularly show Fe and Mn crusting, rip-up clasts are common	Low to moderate undifferentiated bioturbation. Occasional *Planolites*-like and *Thalassinoides*-like
F8 Amalgamated, normal graded mudstone and sandstone	Up to medium-grained, well-sorted to very well-sorted sandstone capped by mudstone	Normal grading	5 to 20 cm	Tabular, amalgamated, occasionally rippled beds with basal scour surfaces	Occasionally contain rip-up clasts	Low to moderate undifferentiated bioturbation. Scarce discrete trace fossils
F9 Deformed, amalgamated mudstone and sandstone	Mixed compositional, up to coarse-grained sandstone capped by mudstone	Normal grading	4 up to 15 cm	Deformed, convolute and/or contorted beds with fluid escape structures	Remnants of original bedding	Low to moderate undifferentiated bioturbation. Scarce discrete trace fossils

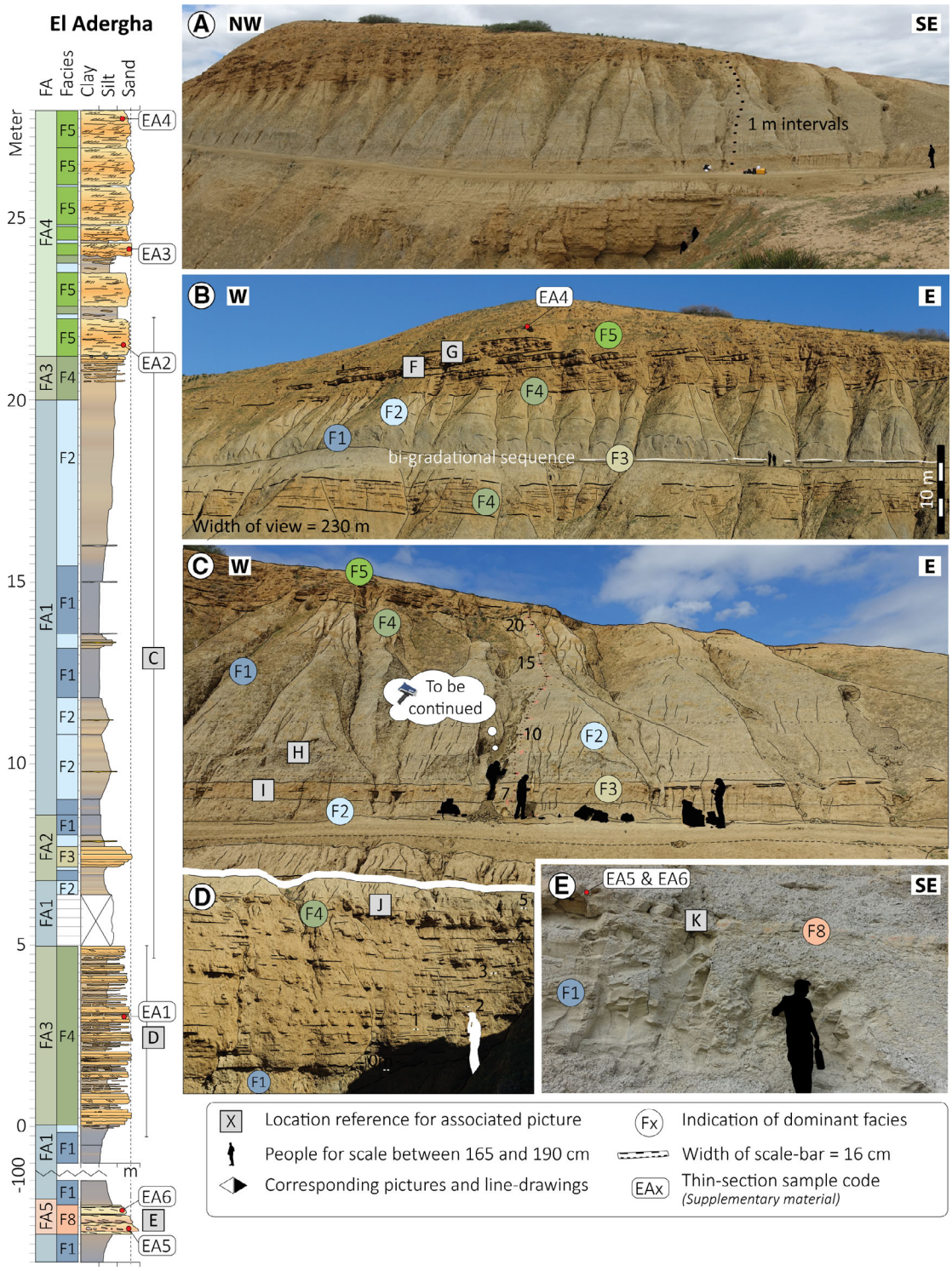

Fig. 7. Sedimentary log for the El Adergha outcrop showing the facies, the facies associations, locations of the samples (Table S1) and the location of the pictures (see legend). (A) Main overview picture of the El Adergha section at an angle perpendicular to the outcrop. (B) Picture perpendicular to part of the outcrop showing facies, reference location of (F) and (G) and the location of sample EA4. (C) Eastward continuation of (B). (D) Lowermost sandstone interval consisting of facies F4 in sharp contact with facies F1. (E) Picture of turbidites stratigraphically located 100 m lower, embedded in the blue marls of facies F1. Collage of examples of facies from the El Adergha outcrop. Picture letters correspond to those in (A) to (E).

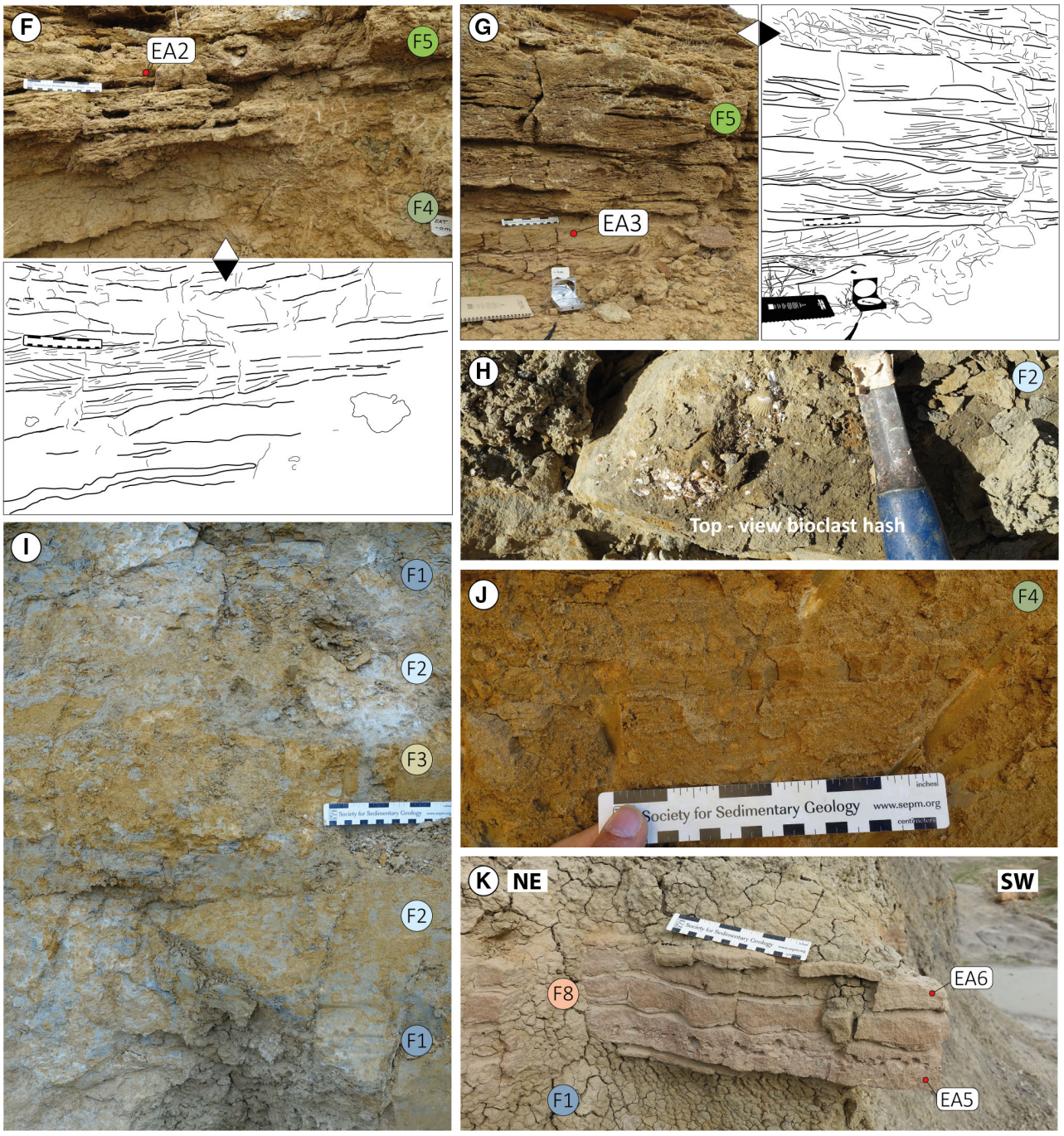

Fig. 7 (continued). (F) Picture and line-drawing of the contact between facies F4 and F5 at 21 m in the log. Facies F4 is mottled, not easily captured by lines at this scale. (G) Picture and line-drawing of typical facies F5. The lowermost right corner is not well-exposed. (H) Top-view picture of bioclast (pecten) hash, imbrication bioclastic material not visible in picture. Note the 1 cm pecten shell in the middle top-view of the picture. (I) Bi-gradational stacking of facies F1–F2–F3–F2–F1. The F3 and F2 facies are intensely bioturbated leaving a mottled appearance. (J) Typical facies F4, consisting of laminated sandstone and mudstone and moderate bioturbation. (K) Turbidite deposits found roughly 100 m stratigraphically below the main studied interval, embedded in facies F1.

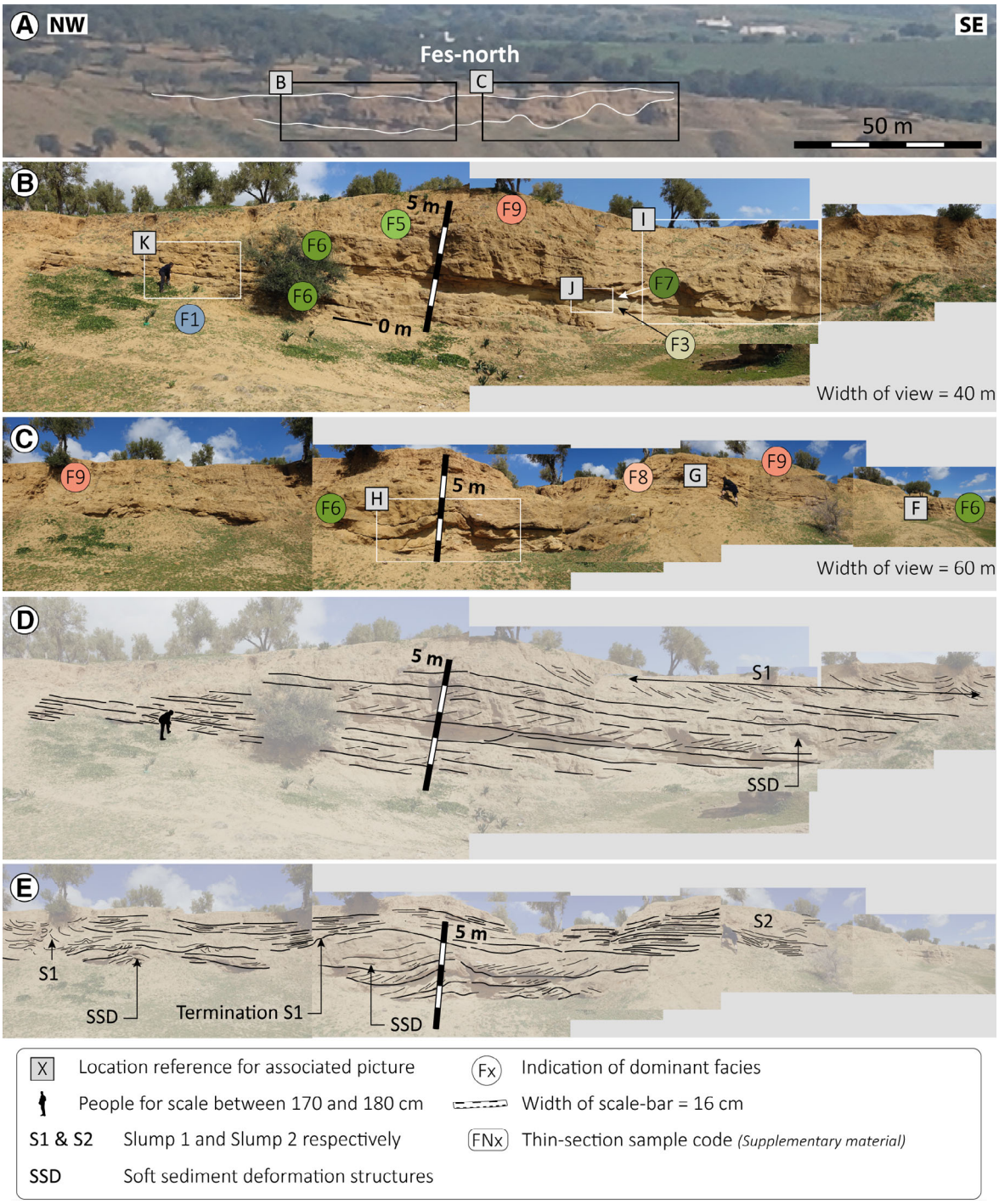

Fig. 8. (A) Panoramic picture of the Fes-north outcrop with the panels indicating the locations of (B) to (E). (B) and (C) form a collage of the laterally (NW–SE) continuous section. Within these pictures the main facies distribution are indicated as well as locations for (F) to (K). (D) and (E) Line-drawings of (B) and (C) respectively. These line-drawings are made to emphasize bed-boundaries and internal structures. (D) Image clearly shows the tectonic tilt of the beds with respect to the near horizontal horizon. At the 5 m mark of the scale bar (4 m in the log) the mainly tabular beds with cross-stratification directed towards the left are overlain by S1 (slump 1) which is stratified mainly in the opposing direction. (E) This eastward lateral and upward continuation of panel D (S1 for reference) shows that lateral facies changes are present. Furthermore, the termination of S1 against facies F6 (C) is visible. Within facies F6 SSD structures are visible. S2 overlies the more planar stratified facies F8 here.

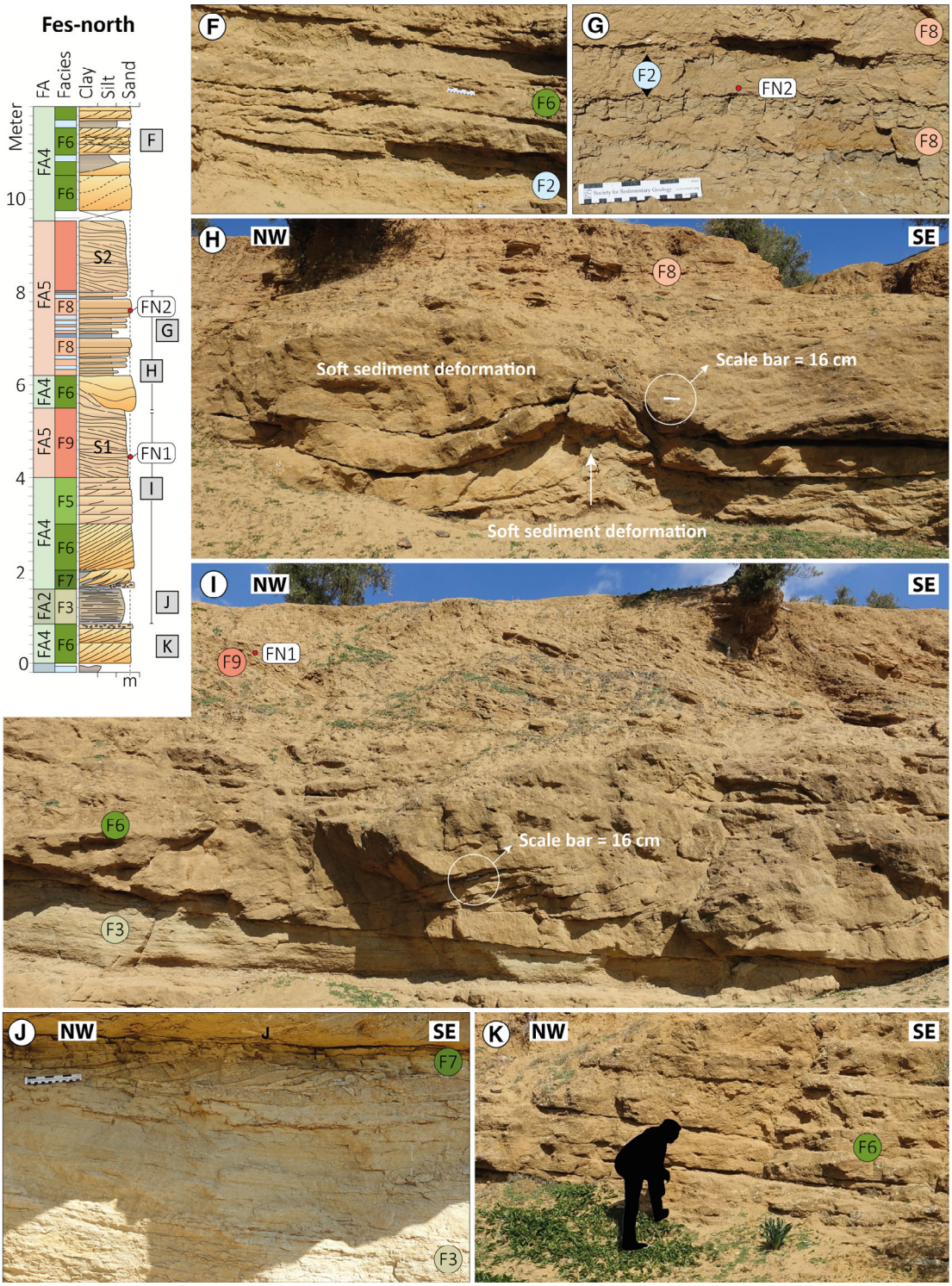

Fig. 8 (continued). Sedimentary log and picture collage of facies in the Fes-north outcrop. (F) Picture of facies F2 and F6, corresponding to 11 to 12 m in the log. Cross-stratification of facies F6 is directed towards the left (west). (G) Facies F8, alternating with facies F2. Facies F2 in this succession represents suspension fallout from a turbidity cloud. (H) Overview picture of the interval between 5.5 m and 8.0 m in the sedimentary log. The lower field of view shows facies F6 containing soft sediment deformation structures. This facies is overlain by facies F8. (I) Overview picture of the interval between 1.0 m and 5.5 m in the log. Here facies F3 and F6 are overlain by slump deposits of facies F9. (J) Picture showing both facies F3 and F7 and their stratigraphic relationship. On top of facies F7 a sharp basal contact with facies F6 is present. (K) Westernmost expression of the exposed outcrop with stacked tabular beds of facies F6.

Facies F1 – Fossil-rich blue marlstone

Description

Facies F1 consists of blueish marls, the sediments after which the Blue Marl Formation is named (Table 1; Fig. 7A to E). The intervals containing these dominantly structureless, fossil-rich marlstones (containing bivalves up to a centimetre in size) range in thickness from decimetres to hundreds of metres forming a continuous succession. Despite being dominantly blueish in colour, modest gradational changes ranging on average from 0.5 to 2.0 m in thickness from dark blueish-grey to more brownish-grey are common. This colour change results from slight increases in the biogenic and siliciclastic fraction consisting of up to fine-grained and very fine-grained sand, respectively. F1 only shows scarce discrete trace fossils.

Interpretation

The late Miocene blue marls of F1, are widely recognized in northern Morocco and other parts of the Mediterranean region where they are generally associated with open deep-marine conditions (DiGeronimo *et al.*, 1981; Bernini *et al.*, 1992; Krijgsman *et al.*, 1999; Mansour & Saint-Martin, 1999; Barbieri & Ori, 2000; Gelati *et al.*, 2000; van Assen *et al.*, 2006; Capella *et al.*, 2017a). F1 represents a low energy depositional environment where sedimentation is dominated by the vertical settling and lateral advection of both fine-grained biogenic and terrigenous particles through the water column, or hemipelagic sedimentation (Hesse, 1975; Stow & Piper, 1984; O'Brien *et al.*, 1991; Einsele, 2000).

The common increases in silt and sand content suggest fluctuations in carbonate productivity, terrigenous sediment supply and/or in the hydrodynamic regime. These alterations in silt and sand content might reflect the presence of low-density turbidity currents (Lowe, 1982), in which case they reflect Bouma divisions Td and Te (Bouma, 1962), diluted gravity flows and/or the activity of weak bottom currents (Stow & Faugères, 2008; Rebesco *et al.*, 2014; Stow & Smillie, 2020).

Facies F2 – Sandy marlstone

Description

Facies F2 consists of fossil-rich sandy marlstone and very fine-grained muddy sandstone (Table 1; Fig. 7C, H and I). This facies occurs over intervals with thicknesses ranging from centimetres to tens of metres. The texture is homogeneous for the finest intervals that are more blueish-grey in colour. The coarser and more light-brownish grey intervals are regularly banded or laminated. Starved ripples of fine-grained sand are scarce. Changes in grain-size distribution are generally gradational, but sharp basal contacts have been observed between muddy and more sandy deposits. Laminae with sharp basal bounding surfaces and ripples coincide with an increased abundance of fine-grained, imbricated shell fragments (Fig. 7I) indicating palaeo-flow directions towards the west. The muddier intervals regularly contain well-preserved bivalves up to 1.5 cm in diameter. The trace fossil assemblage consists of abundant undifferentiated structures and scarce *Planolites*-like and *Thalassinoides*-like traces (Fig. 9A and C).

Interpretation

Facies F2 represents a sand-enriched equivalent of facies F1, reflecting deposition under higher-energy conditions and/or a change in sediment supply. This facies generally lacks sharp bounding surfaces and traction structures, although the presence of the occasional bioclast enriched laminae may represent the remnants of traction carpets. Furthermore, the occasionally observed sharp lower bounding surfaces and sand lenses, which are likely remnants of starved ripples, rule out a pure hemipelagic origin.

Since sedimentary structures and other features related to turbiditic processes are lacking, it is likely that the change in sediment supply primarily resulted from hemipelagic settling of a turbidite suspension cloud also known as a hemiturbidite (Stow & Wetzel, 1990). However, the gradual (consecutive inverse and normal-graded) trends in grain-size distribution might reflect the presence of – and subtle changes in – bottom current velocities (Gonthier *et al.*, 1984; Hüneke *et al.*, 2020).

If hemiturbiditic processes were active, bottom currents, induced by the palaeo-MOW, likely deflected the turbidite suspension cloud downcurrent, changing the orientation from downslope to along-slope. This deflection might be inferred from occasionally occurring imbrication patterns of shells and subtle ripple laminae. Furthermore, bottom currents might have been able to winnow and rework the sediment, preventing the settling of the finest particles in the coarsest intervals of facies F2. Winnowing and reworking can also be used to explain the occasional sharp bounding surfaces that are regularly interpreted to result from peak current velocities in most

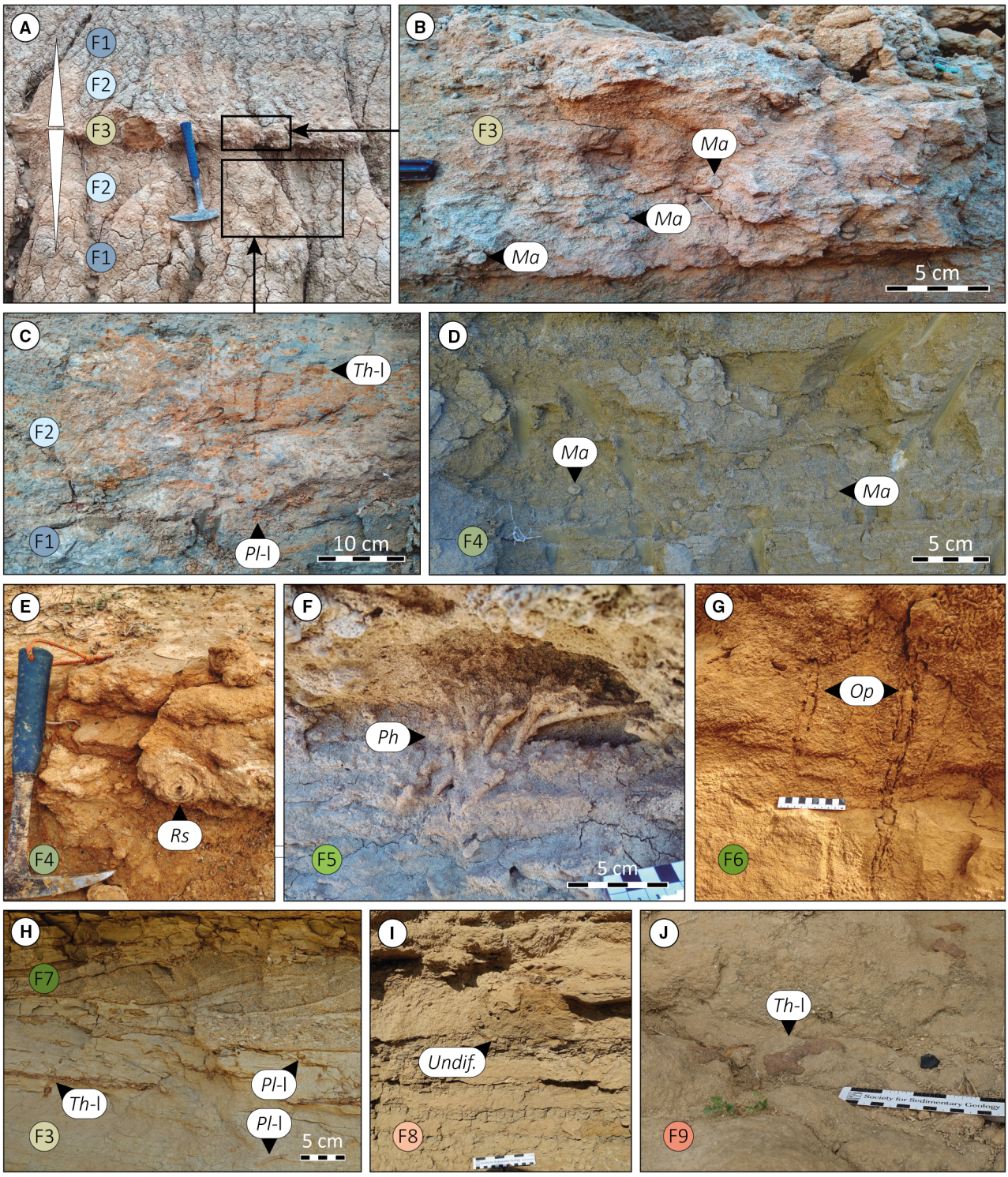

Fig. 9. Overview of recognized ichnospecies: *Macaronichnus (Mn)*, *Thalassinoides (Th)*, *Planolites (Pl)*, *Rosselia (Rs)*, *Ophiomorpha (Op)* and undifferentiated (Undif.) traces. The addition of (l) stands for '-like'. Facies are indicated with the coloured and labelled circles. (A) to (F) are taken from the El Adergha sections and (G) to (J) from the Fes-north section.

environments affected by bottom currents (Lucchi & Rebesco, 2007; Martín-Chivelet *et al.*, 2008; Rebesco *et al.*, 2014; de Castro *et al.*, 2020a,b).

Based on available data, it is hypothesized that the subtle compositional changes in facies F2 are the result of the interaction between hemipelagites, low-density turbidites and weak bottom currents. Fluctuations in the bottom current activity related to intensification and weakening of the palaeo-MOW might have reworked initial turbidite deposits and have caused fluctuations between contouritic and hemipelagic dominated periods. Based on grain-size, depositional texture and according to the bedform-velocity matrix proposed by Stow *et al.* (2009), bottom currents never exceeded 20 to 25 cm s^{-1}. Similar facies have recently been identified in the proximal and central sectors of the Gulf of Cadiz CDS, where muddy contourites are usually interbedded with hemipelagites and turbidites, forming metre-scale sedimentary deposits (de Castro *et al.*, 2020b).

Facies F3 – Bi-gradational sandstone

Description

Facies F3 consists of an inverse to normal-graded sandstone with a thickness ranging from 10 to 60 cm (Table 1; Figs 7B, 7J and 8J). This bi-gradational pattern consists of very fine-grained, fine-grained and up to medium-grained sand. The sand is of mixed bioclastic–siliciclastic composition (Chiarella *et al.*, 2017). Between the El Adergha and Fes-north section, differences in this facies have been observed.

In the El Adergha section, facies F3 (Fig. 7B) is more bioclastic, contains glauconite and abundant bioturbation of *Macaronichnus* (Fig. 9A and B), rare *Planolites*, *Thalassinoides* and *Rosselia* (Fig. 9E), leaving a severely bioturbated appearance (Fig. 7J). However, despite the intense bioturbation, planar erosive surfaces between the inverse-graded and normal-graded division have been recognized in places. In the Fes-north section, F3 consists of distinct planar laminae with the thickest laminae (up to 1.5 cm) coinciding with the coarsest (medium-grained) sand fraction (Fig. 8J). Biogenic structures are limited to a low to moderate number of undifferentiated burrows, and scarce *Planolites and Thalassinoides*-like traces (Fig. 9H).

Interpretation

The bi-gradational sandstone of facies F3 in the El Adergha section very closely resembles the C3 division of the bi-gradational contourite facies model proposed by Faugères *et al.* (1984), Gonthier *et al.* (1984) and Stow & Faugères (2008). The very close resemblance of this bi-gradational facies to the C3-division of the 'diagnostic contourite facies model' favours the interpretation of a contouritic drift origin. This interpretation is supported by the findings of Capella *et al.* (2017a).

Bi-gradational sequences, however, might also be formed in different types of current-influenced depositional settings where waning/waxing currents are common, such as deltas with fluctuating river discharge. There is however no evidence of such current-influenced depositional systems in the surrounding area for the depositional period between 7.51 Ma and 7.25 Ma. Furthermore, the lack of distinct erosional surfaces both below and above facies F3 in the El Adergha section (Fig. 7I) indicates subtle changes in the depositional setting and thus the depositional domain did not significantly change to that inferred from the benthic foraminifer assemblage for facies F1 (i.e. the continental slope). This thus suggests that facies F3 was formed in the slope depositional domain, a common area for the formation of contourite drift deposits (Faugères *et al.*, 1999; Hernández-Molina *et al.*, 2008; Rebesco *et al.*, 2014).

Despite the slight differences in facies F3 observed between both outcrops, subtle breaks in sedimentation, indicated by the style of bioturbation and the relatively sharp bounding surfaces in the El Adergha and Fes-north sections, respectively (Figs 7I and 8J), show that the long-term flow fluctuation responsible for the bi-gradational sequence, was also affected by shorter scale flow variations. These shorter scale variations indicate that, at times, flow velocities were sufficiently high to cause a break in sedimentation, and/or there was a break in sediment supply. Omission surfaces in the central part of the bi-gradational sequence have previously been reported in similar sequences, interpreted as contourite drift deposits, from the ancient record (Rodríguez-Tovar *et al.*, 2019; Hüneke *et al.*, 2020).

Facies F4 – Heterolithic, thin-bedded mudstone and sandstone

Description

Facies F4 consists of heterolithic orange to reddish-grey clay and marlstone and brownish to orangish-grey very fine-grained up to medium-grained sand (Table 1; Fig. 7J). The finely laminated to thinly bedded sands (<10 cm) are

tabular (Fig. 7D) and occasionally show ripples. The base of the sandstone beds is sharp or gradational and occasionally shows an undulatory geometry. The sand component is of mixed siliciclastic–bioclastic composition, enriched in glauconite (<10%). Muddy laminae that are interbedded with the sands, are often wavy, lenticular or discontinuous parallel. Other features include silty mud flasers and muddy rip-up clasts (Fig. 7F and J). A mottled appearance, predominantly concentrated in the finest sediments, results from intense, often undifferentiated bioturbation. The trace fossil assemblage consists of abundant *Macaronichnus* (Fig. 9D), common *Parahentzschelinia* and rare *Planolites, Rosselia* (Fig. 8E) and *Thalassinoides*.

Interpretation

Facies F4, in comparison to facies F1 and F2, due to its coarser medium grain-size and the presence of occasional traction structures, is related to higher peak current velocities. As this facies unconformably overlies facies F1 and F2 (Fig. 7D and B, respectively), it indicates a change in hydrodynamic conditions related to an increase in maximum flow velocity. Like facies F3, the depositional domain was likely in the slope, ruling out a shallow-marine current-dominated setting. The rhythmical variations in grain-sizes and co-occurrence of fine-grained sand and mud laminae suggest deposition through alternating periods of bedload and suspension transport. Since facies F4 closely resembles the stacked sand sheets described by Martín-Chivelet *et al.* (2008), Rebesco *et al.* (2014), de Castro *et al.* (2020a) and Hovikoski *et al.* (2020) it might have a similar origin related to bottom currents with alternating flow conditions. During peak current velocities, the fine-grained sand can form ripples whilst the finest fraction of the sediment is winnowed or re-incorporated as aggregates and rip-up clasts (de Castro *et al.*, 2020a). Hüneke *et al.* (2020) suggest that fluctuating bottom currents characterize deposition for all contourite divisions even though the controlling mechanism behind the short-term fluctuation of flow strength is unknown. Shanmugam (2008), however indicated that short-term oscillating energy conditions have been described from thermohaline and wind-driven bottom currents. Furthermore, climatic and tidal induced changes on the characteristics of the palaeo-MOW also affect variability in flow-conditions on shorter, millennial to sub-annual timescales (de Castro *et al.*, 2020b; de Weger *et al.*, 2020). These processes explain the development of heterolithic alternations as a consistent indicator of bottom current fluctuations. The preservation of primary sedimentary structures within the sandstone beds indicates that bottom currents remained sufficiently strong to winnow away fine-grained sediment and to prevent disruption due to bioturbation (de Castro *et al.*, 2020a).

Facies F5 – Heterolithic, cross-stratified mudstone and sandstone

Description

Facies F5 typically consists of heterolithic, dominantly thin-bedded (<10 cm) to medium-bedded (<20 cm) sandstones draped by mud (Table 1; Fig. 7G and H) that are part of large westward migrating foresets (Fig. 7B). These beds, which thus likely present foresets, show unidirectionally westward verging cross-strata (Fig. 7C) with bundles of thickening and thinning foreset-laminae and angular to tangential toe-set geometries (Figs 7G and 10A; more clearly visible in 10A). Beds form 1.0 to 1.5 m thick sets, associated with the previously mentioned westward migrating foresets. Cross-sets have a planar parallel to undulatory erosive base and regularly show traction carpets of muddy rip-up clasts and small (centimetre-scale) scours at their base (Fig. 7G). The beds occasionally contain ripples showing opposing current directions (Fig. 7G). The sand consists of fine-grained up to coarse-grained sand of orangish-brown colour. Bed boundaries regularly show Fe-Mn crusting. Biogenic structures are dominantly vertically oriented and consist of an assemblage of abundant *Parahaentzschelinia* (Fig. 9F) and *Macaronichnus*, common undifferentiated vertical structures, and rare traces such as *Ophiomorpha*-like and *Skolithos* vertical traces.

Interpretation

The cross-stratified nature and general tabular bedding of these westward migrating deposits suggests them to be relics of deep-marine two-dimensional (2D) dunes. Based on the presence of thickening and thinning foreset-bundles (Allen, 1982; Longhitano & Nemec, 2005), gradual changes between angular to tangential toe-set geometries (Chiarella, 2016; Fig. 10) and sand–mud couplets (Nio & Yang, 1991; Longhitano *et al.*, 2012), the formation of these deposits was influenced by oscillatory flow. As such, this facies can be related to a tidally modulated current.

Facies F5, based on dominant palaeocurrent directions indicating westward flow, is

interpreted as a relic of westward migrating dunes. This interpretation is supported by the findings of Capella *et al.* (2017a). These dunes migrated under current velocities reaching more than 1 m s^{-1} (Stow *et al.*, 2009) in a late Tortonian channel in front of a strait. These conditions infer a depositional environment where energy is more concentrated than in other sectors, such as the contourite channel. Similar sandy deposits have also been identified in modern contouritic channels (Nelson *et al.*, 1993, 1999; Hernández-Molina *et al.*, 2006, 2014b; Stow *et al.*, 2013; Brackenridge *et al.*, 2018; Lozano *et al.*, 2020). The dominance of vertical biogenic structures in F5 supports the occurrence of energetic environmental conditions.

Facies F6 – Cross-stratified sandstone

Description

Facies F6 consists of sandstones with unidirectionally westward verging cross-strata which include bundles of thickening and thinning foresets that show alternations between angular to tangential toe-set geometries (Fig. 8D, F and K). Bedding is generally 10 to 100 cm thick and has sharp basal boundaries with common muddy rip-up clasts. The thickest beds have a subtle concave-up geometry. Sediment is composed of moderately to well-sorted, medium-grained to coarse-grained sand represented by mixed bioclastic–siliciclastic grains. This facies is moderately bioturbated with *Ophiomorpha* (Fig. 9G), occasional *Skolithos* and rare *Planolites*, *Rosselia*-like and *Thalassinoides* trace fossils. Sometimes burrow linings as well as bed boundaries show Fe-Mn crusting.

Interpretation

Like facies F5, the cross-stratified nature and the presence of tidal signatures of these westward migrating deposits (Fig. 5) suggests them to be relics of deep-marine 2D dunes the formation of which relies on a tidally modulated current near the seafloor. The lack of mud drapes indicates that, despite the tidally modulated alternating flow conditions, flow velocities never dropped below the threshold value to deposit and/or preserve muddy sediment, indicating that deposition took place under flow velocities ranging from *ca* 50 cm s^{-1} to over 1 m s^{-1} (Stow *et al.*, 2009). These conditions also infer a depositional environment in the slope domain where energy is more concentrated than in other sectors, such as the contourite channel. Like facies F5, similar sandy deposits have also been identified in modern contouritic channels (Nelson *et al.*, 1993, 1999; Hernández-Molina *et al.*, 2006, 2014b; Stow *et al.*, 2013; Brackenridge *et al.*, 2018; Lozano *et al.*, 2020). The dominance of vertical biogenic structures in facies F6 also supports energetic environmental conditions.

Facies F7 – Sigmoidal, mud-draped sandstone

Description

Facies F7 consists of sigmoidal cross-stratified sandstone alternating with mudstone (Table 1). The sandstone foresets are encapsulated in and draped by up to 1 cm thick, scarcely bioturbated mud forming distinct up to 30 cm thick bundles of thickening and thinning foresets (Fig. 8J). Muddy to marly rip-up clasts are common and mainly occur at the basal bounding surfaces. The sand fraction consists of up to granule-sized mixed siliciclastic–bioclastic sand. Biogenic structures are limited to scarce discrete trace fossils (for example, *Thalassinoides*-like and *Planolites*-like).

Interpretation

The sand–mud couplets recognized in the cross-strata of facies F7 suggest a fluctuation in the energy of the flow to form heterolithic bundles. The mud drapes and ripped-up muddy clasts are thought to represent fine particles originating from high suspended mud concentrations (Faas, 1991). Accordingly, the sandy intervals represent the record of current-dominated processes while the draping mud reflects a moment of reduced energy, favouring the decantation and drapes of the fine-grained material previously kept in suspension (Visser, 1980). According to Nio & Yang (1991), a bimodal grain-size with the muds interlayering medium-grained or coarse-grained sandstones is an indication of tide-modulated currents. The lack of sedimentary structures referable to wave action and high-energy environments suggest a depositional environment below the fair-weather wave base in a current-dominated environment.

Facies F8 – Amalgamated, normal graded mudstone and sandstone

Description

Facies F8 consists of heterolithic mudstone and sandstone intervals (Table 1; Figs 7K and 8G). The tabular, generally thin-bedded, sandstones (up to 20 cm) are normal graded, and regularly

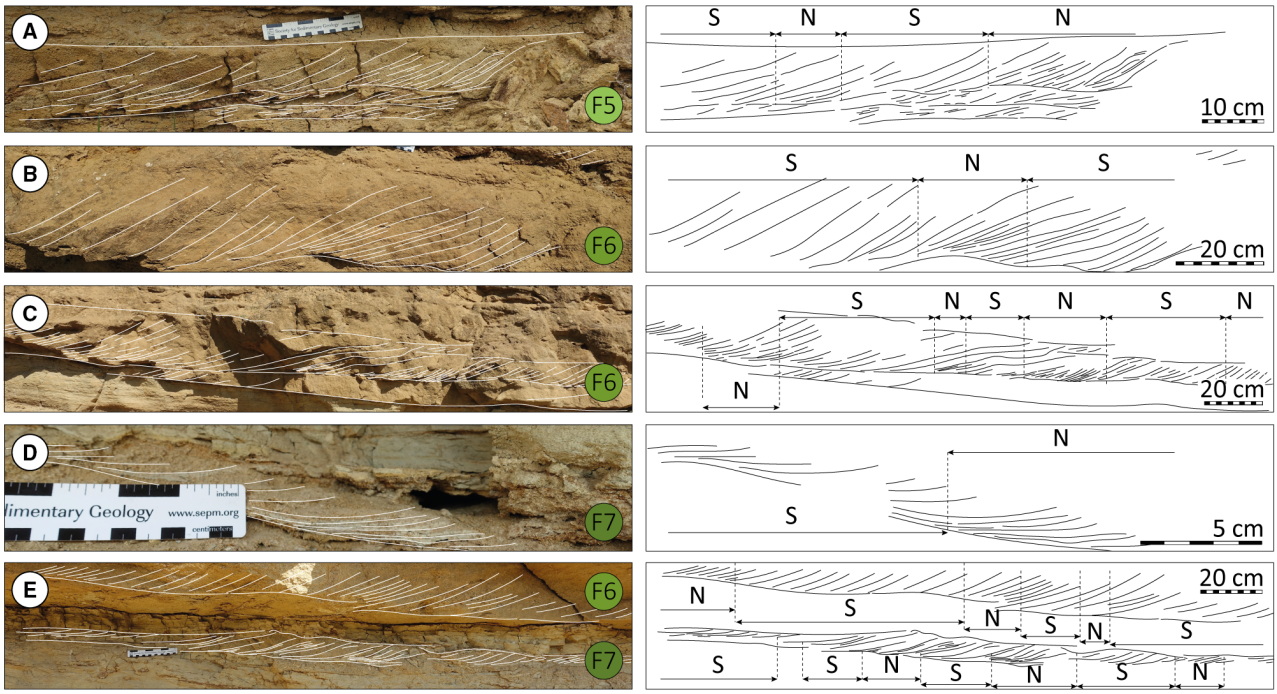

Fig. 10. Examples of cyclic thickening and thinning foreset intervals and cyclic alterations between angular and tangential toe-sets. These alternations are associated with cross-stratification and interpreted as the record of sandy bedforms migrating under unidirectional, tidal-modulated accelerating/decelerating currents. N = neap tide; S = spring tides.

have small (centimetre-deep) basal scours. Although a semi-gradational transition from sand to mud occurs, boundaries can be easily distinguished. This facies in El Adergha, consists of thin, amalgamated beds presenting basal rip-up clasts of up to pebble sized marls, plane-parallel lamination and ripples, capped by a very thin marlstone. The sediment is of mixed siliciclastic–bioclastic composition. The sand is up to medium-grained and well-sorted to very well-sorted. The facies is bioturbated with scarce undifferentiated discrete trace fossils (Fig. 9I).

Interpretation

Facies F8 generally shows basal scours and clear bounding surfaces. The well-sorted to very well-sorted, normal graded beds and internal structures typically represent a decelerating turbulent flow from the upper flow regime to suspension fallout (Bouma, 1962) and are, as such, interpreted as turbidites. The sediment composition of the sand fraction in this facies varies between both the El Adergha and Fes-north sections (Fig. 10B to D). At the El Adergha section, facies F8 consists of very fine-grained, relatively mature siliciclastic sand whereas at the Fes-north section, it consists of medium-grained, immature siliciclastic sand (Table S1; Fig. S2). This implies that facies F8 at the El Adergha section represents a more distal sector in respect to the Fes-north section. The composition and stacking pattern of facies F8 in El Adergha (Fig. 7K) is most like those observed in base-of-slope or basin wedge settings (Stow, 1985). The tabular thin bedded nature of facies F8 recognized in the Fes-north section (Fig. 8C, G and H) might also suggest a basinal turbidite (silty–sandy distal lobe) depositional setting. However, here facies F8 more likely represents the tail of turbidity current deposits on the slope (Mutti, 1992; Mutti *et al.*, 2009; Mulder, 2011; Talling *et al.*, 2012) or very low-density turbiditic currents on the slope as recently discussed by de Castro *et al.* (2020a,b) and Hüneke *et al.* (2020).

Facies F9 – Deformed, amalgamated mudstone and sandstone

Description

Facies F9 consists of amalgamated, heterolithic, thin-bedded (up to 10 cm) strata of marlstone and

sandstone up to medium-grained (Table S1; Fig. S2A). Strata are convolute and fluid escape structures are common (Fig. 8B, C and I). The primary sedimentary structure is like facies F8, consisting of amalgamated normally graded tabular, thin-bedded mudstone and sandstone. The base is sharp, erosive and in many cases seems to have deformed the underlying facies (Fig. 8H). This facies appears wedge shaped, thinning out northwestward. The preserved primary bedding is folded, indicating south to south-eastward deformational migration. Inclination of the modified but preserved primary strata varies laterally from high-angle (40°, westward dipping) to opposing angles (20°, eastward dipping) (Fig. 8D and I). Biogenic structures are scarce and discrete trace fossils are difficult to identify, a few *Planolites*-like traces were observed (Fig. 9J).

Interpretation

The convolute and/or contorted nature, accompanied by the erosive basal surface recognized in facies F9 suggest that it represents the product of a slump (Leeder, 2009; Reading, 2009; Shanmugam, 2010). Additional evidence of the sudden displacement of large volumes of sediment is found in the fluid-escape structures locally present in the underlying sediment. Although slumps may occur over a wide range of depositional environments, their formation relies on slopes. Since the primary bedding of facies F9 is like F8, F9 represents down-slope, plastically deformed fine-grained turbidites.

Ichnofacies

Ichnological analysis from the El Adergha and Fes-north sections reveals, in general, low ichnodiversity in assemblages. El Adergha has a higher abundance of traces which are dominantly horizontal whereas the structures in Fes-north are dominantly vertical. This difference is related to variable palaeoenvironmental conditions, especially with respect to hydrodynamic energy.

The trace fossil assemblages at the El Adergha section are characterized by low ichnodiversity and a high abundance of traces produced by deposit feeders. The two main ichnogenera (*Macaronichnus* and *Parahaentzschelinia*) are typical of proximal, shallow marine environments related to the *Skolithos* ichnofacies (MacEachern *et al.*, 2007, 2012; Buatois & Mángano, 2011; Knaust, 2017). However, being typified by dominantly horizontal traces allows assignation to the *Cruziana* ichnofacies which is typical of deeper and more distal environments. In this context, the presence of vertical structures could be related to periods with stronger bottom currents creating higher energetic palaecological conditions like those in shallow marine environments (i.e. upper slope) at more distal and deeper settings (Miguez-Salas *et al.*, 2020).

In the Fes-north section, trace fossil assemblages record low ichnodiversity and a moderate to low abundance of traces of dominantly vertical forms. The main ichnogenus is *Ophiomorpha*. *Ophiomorpha* is generally, but not exclusively, characteristic of high-energy environments (i.e. shoreface) with well-sorted shifting sandy substrates, constituting a typical element of the *Skolithos* ichnofacies (MacEachern *et al.*, 2007, 2012). However, the appearance of *Ophiomorpha* in deep-sea environments with gravity flow sediment supplies confirms the *Ophiomorpha rudis* ichnosubfacies (Uchman, 2009, and references therein). Thus, the presence of *Ophiomorpha* should not necessarily be related to the *Skolithos* ichnofacies, but to higher energetic environments at Fes-north than that corresponding to El Adergha.

DEPOSITIONAL SUB-ENVIRONMENTS

Depositional elements and facies associations

The sedimentary facies are linked to form distinct facies associations (FA) and depositional elements (Table 2). The fine-grained sediments of facies F1 and F2 are grouped into FA1. FA1 occurs over intervals of one to hundreds of metres thick where both facies regularly grade into one another. FA1 is generally coarsening-upward grading from facies F1 to F2. FA2 consists of the distinct bi-gradational stacking of facies F1, F2, F3, F2 and F1 (Fig. 7J) or F2, F3 and F2 (Fig. 8J). FA3 consists of facies F4, which, albeit heterolithic, is considered an individual facies based on the regular lack of bounding surfaces. However, the heterolithic occurrence of sandstone and marlstone could be considered the alternation between fine-grained facies (F1 and F2) and sand-rich facies somewhat similar in sedimentary composition as facies F3. FA4, consisting of facies F5, F6 and F7, typified by the presence of traction structures (mainly cross-stratification). FA5 is distinguished based on depositional features with palaeo-transport indicators perpendicular (down-slope) to those observed in FA4.

Based on the: (i) palaeogeographic reconstruction of the South Rifian Corridor; (ii) the topography of the Prerifian Ridges on the northern margin of this corridor (Fig. 6); (iii) the interpretation that the studied sections have been deposited in a slope depositional domain; and (iv) evidence suggesting the presence of a late Miocene unidirectionally westward migrating, tidal influenced bottom current (Fig. 10), it is suggested that the studied sedimentary successions were formed predominantly by the action of the late Miocene palaeo-MOW. As such, the facies associations and depositional domains are interpreted within this framework (Fig. 11).

Fine-grained marine sediment (FA1)

Based on the available data, the fine-grained marine sediment of facies association FA1 and its subtle changes in composition is interpreted to result from the interaction between hemipelagic, low-density turbiditic and bottom current induced sedimentation. Fluctuations in the bottom current activity, related to the intensification and deceleration of the palaeo-MOW have primarily caused fluctuations between contouritic and hemipelagic dominated periods. Similar facies have recently been identified in the proximal and central sectors of the Gulf of Cadiz CDS where muddy contourites, associated with the drift, are usually interbedded with hemipelagites forming metre-scale sedimentary deposits (de Castro *et al.*, 2020b). As such, facies association FA1 has been interpreted to represent the contourite drift or a zone that is located even more distally, further down the slope (Fig. 12).

Contourites: drift-channel transitional deposits (FA2 and FA3)

Both facies associations FA2 and FA3, due to their relative increase in grain-size and the presence of subtle indicators of bedload transport, are indicative of higher bottom current velocities compared to facies association FA1. This suggests an increase in the palaeo-MOW activity. However, the heterolithic occurrence of sand and mud indicates fluctuating energy conditions.

The strength or velocity of bottom currents associated with overflow water decreases both laterally and down current of the core of the bottom current which is generally confined to a contourite channel (Fig. 11) (McCave & Tucholke, 1986; Faugères *et al.*, 1999; Llave *et al.*, 2001; Rebesco *et al.*, 2014; de Castro *et al.*, 2020b). The core of the current is influenced by the Coriolis force. In the case of this study, the westward flowing palaeo-MOW was forced towards the right (north) against the north–south oriented palaeo-slope of the northern margin of the South Rifian Corridor (Fig. 11).

Since the highest bottom current velocities are associated with the contourite channel and the weakest bottom currents to the drift (Fig. 12), both facies associations FA2 and FA3 represent a transitional depositional environment with weaker currents compared to the core and stronger currents compared to the drift. Facies like those described in facies associations FA2 and FA3 have recently been ascribed to a drift-channel transitional domain where energy conditions are slightly higher than in the drift due to the increased influence of the more closely

Table 2. Sedimentary facies associations (FA) established for sedimentary deposits in the El Adergha and Fesnorth outcrops.

Sediment size	Orientation	Facies association	FA	Dominant facies	Thickness (m)
Fine-grained sediment	Vertical settling, along-slope and down-slope	Contourite drift	FA1	F1 – *Hemipelagites* F2 – *Fine-grained turbidites or contourites*	up to 100s
Coarse-grained sediment	Along-slope	Drift/channel transition	FA2	F3 – *Fine-grained sandy contourites*	0.6 to 1.5
		Channel/drift transition	FA3	F4 – *Bottom current reworked sands*	0.1 to 5.0
		Contourite channel	FA4	F5, F6 and F7 – *Coarse-grained sandy contourites*	0.2 to 5.0
	Down-slope	Upper slope	FA5	F8 – *Turbidites* F9 – *Slumped deposits*	0.1 to 2.0

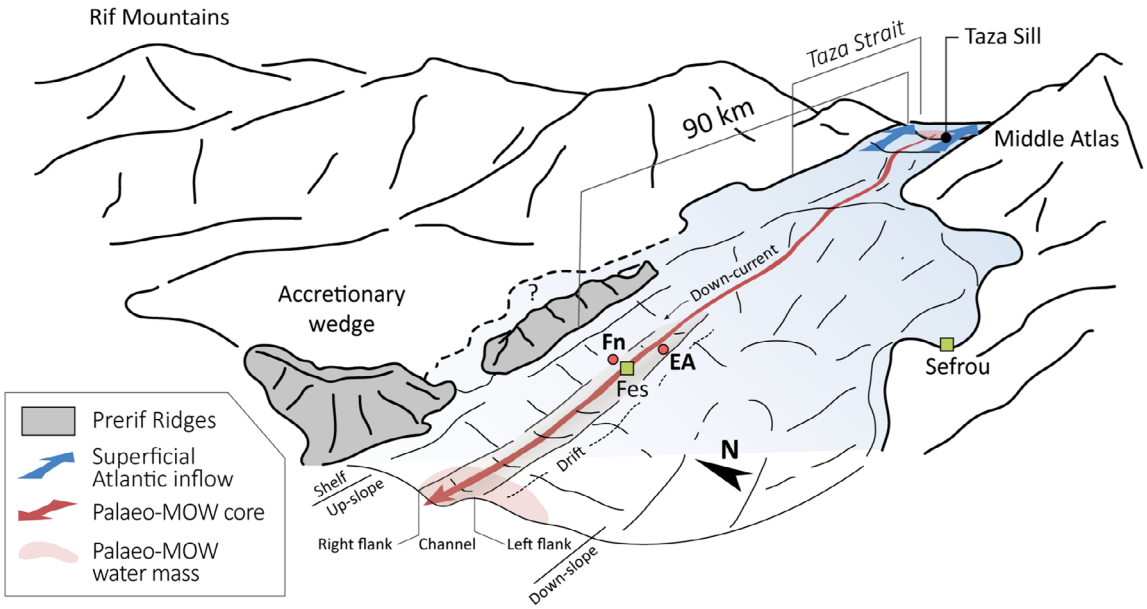

Fig. 11. Palaeogeographic reconstruction of the late Miocene Rifian corridors between 7.51 Ma and 7.25 Ma. The palaeo-Mediterranean Outflow Water (palaeo-MOW) cascaded over the Taza Sill, through the Taza Strait into the South Rifian Corridor where it was forced against the northern margin by the Coriolis force. The Atlantic surficial water flowed through the South Rifian Corridor and Taza Strait into the Mediterranean. The studied sections, Fes-north (FN) and El Adergha (EA) were located closely to or within the contourite channel changing over time. The red arrow, indicating the core of the palaeo-MOW depicts the trajectory of highest current-velocities confined within the channel, whereas the palaeo-MOW water mass was less confined.

located core of the bottom current (de Castro *et al.*, 2020b). Also, areas closer to the core of the bottom current are more strongly receptive to changes in the palaeo-MOW activity, explaining the fluctuating energy conditions.

Contourites: channel fill deposits (FA4)

Facies pertaining to facies association FA4 (F5, F6 and F7) are characterized by a unidirectional trend of palaeo-current indicators showing a direction perpendicular to the north–south oriented palaeo-slope (Figs 11 and 12), indicating a roughly 90° offset compared to those measured in facies association FA5 (Fig. 5). As facies association FA4 shows a slope-parallel trend of dune migration related to high energetic conditions, this facies association is ascribed to the contourite channel.

The differences in sedimentary composition and structures between F5, F6 and F7 can be explained by their relative position within the contourite channel. As mentioned previously, the current velocity decreases away from the core of the bottom current which is also the case within the contourite channel. The palaeo-MOW core was forced northward by the Coriolis force, against the palaeo-slope and therefore towards the slope side of the contourite channel (Figs 11 and 12). This implies that the strength of the bottom current weakens within the channel towards the distally/deeper located drift, but also towards the slope because of increased shear stress. In this case the coarsest sediment related to facies F6 and F7 would be expected in the section closest to the Prerifian Ridges, Fes-north (Fig. 11) if both of the channel facies are related to the same channel. Furthermore, as mentioned in de Weger *et al.* (2020) the palaeo-MOW was intermittent on tectonic, orbital, climatic and tidal timescales. The explanation of processes behind changes in the modern MOW have recently been described by Sierro *et al.* (2020) who found that the MOW strength is mainly driven by precession cycles and the associated freshwater input in the Mediterranean. A decrease in Mediterranean freshwater input during precession maxima results in an increase in Mediterranean salinity and thus Mediterranean deep-water formation. Enhanced, dense Mediterranean deep-water formation results in higher density gradients with Atlantic water and an enhanced, or stronger, palaeo-MOW. On a millennial scale, the study found that Greenland stadials have a positive effect on

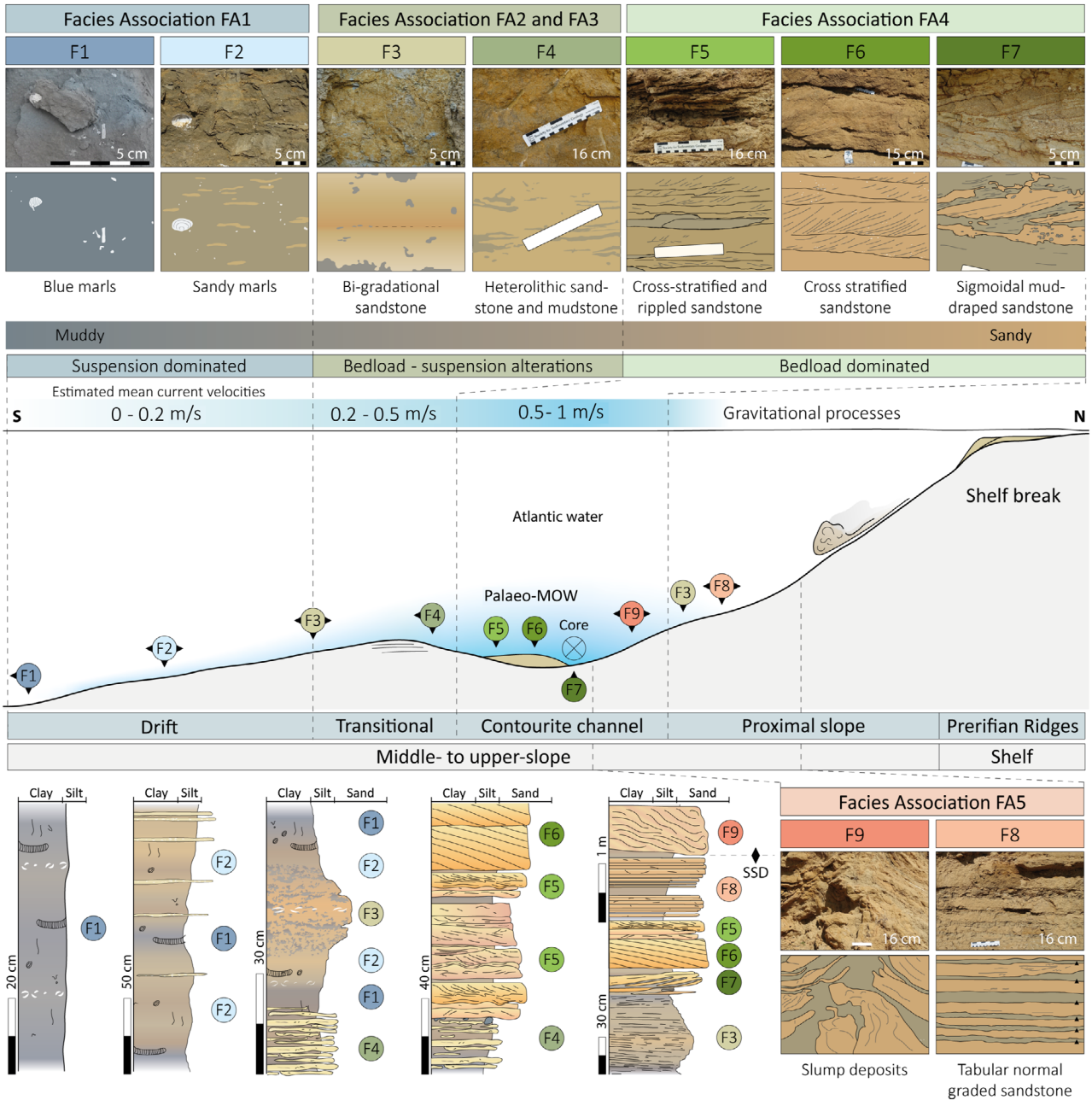

Fig. 12. Sketch showing the relation between the facies (F1 to F9), facies associations and the different depositional and erosional elements from the proximal continental slope to the contourite drift. The facies associations are related to their dominant depositional process and associated current velocities. The panels in the bottom left corner show examples of observed facies stacking patterns. Soft sediment deformation structures (SSD) are regularly observed below facies F9.

buoyancy loss in the eastern Mediterranean which enhances the density gradient with Atlantic water. This results in a more vigorous palaeo-MOW. Similar controlling factors resulted in palaeo-MOW expansion (intensification) and collapse (deceleration) but also in its longer period (> seasonal) oscillatory flow behaviour. Expansion and collapse of the palaeo-MOW likely played an important role in the facies differences of FA4, where, during the deposition of facies F6 and F7, the palaeo-MOW was stronger compared to F5. However, during

the deposition of facies F5 and F7 the palaeo-MOW intensity fluctuated considerably more on tidal timescales. The heterolithic nature within these facies, mudstone and sandstone, is likely related to tidally induced flow acceleration and deceleration where the flow velocity within the channel most significantly decreases towards the channel flanks (F5 and F7) with a decelerating bottom current core.

Gravity-driven flow deposits (FA5)
As mentioned previously, facies association FA5 is characterized by facies with a dominant downslope, north–south oriented, migration component. This down-slope migration is induced by gravitational processes, which, due to these facies occurring interbedded with facies association FA4, indicated that the sections have been deposited on the slope (Fig. 12).

DISCUSSION

Required two-way exchange

The South Rifian Corridor is regularly considered the last remaining gateway before the onset of the Mediterranean Salinity Crisis, yet the termination of Atlantic–Mediterranean connection through the Betic corridors is not fully constrained. Although the Atlantic–Mediterranean connection through the Betic corridors (Fig. 1) largely came to a halt in the late Miocene: (i) the North Betic Strait records continental deposits at *ca* 7.6 Ma (Krijgsman *et al.*, 2000); (ii) the Granada Basin demonstrates a phase of evaporite precipitation between 7.37 Ma and 7.24 Ma (Corbí *et al.*, 2012); and (iii) the Guadix Basin was blocked by 7.8 Ma (Betzler *et al.*, 2006); (iv) the Guadalhorce Corridor might have accommodated Mediterranean outflow until 6.3 Ma (Martín *et al.*, 2001). Furthermore, the possible role of the Strait of Gibraltar in late Miocene Atlantic–Mediterranean exchange should also be considered (Krijgsman *et al.*, 2018) but there is no evidence of its role in connecting both basins between 7.8 Ma and 7.25 Ma.

The Betic corridors were subject to tectonic uplift at around 7.8 Ma (Betzler *et al.*, 2006; Krijgsman *et al.*, 2006), roughly 800 kyr earlier than in the Rifian corridors where tectonic uplift was initiated around 7 Ma (Capella *et al.*, 2017b; Tulbure *et al.*, 2017). This suggests that the Betic corridors were shallowing long before the Rifian corridors. By means of physical modelling, de la Vara *et al.* (2015) demonstrated that the exchange through the Betic – Guadalhorce Corridor and the South Rifian Corridor depends predominantly on the depth of each corridor with respect to the other. More specifically, both corridors present two-way flow unless the shallower gateway is shallower than about the mid-depth of the deeper corridor. Based on the Guadalhorce Corridor having been affected by tectonic uplift prior to the South Rifian Corridor, it is very likely that the South Rifian Corridor, or more specifically the Taza Sill, was twice as deep, only allowing two-way exchange through the Taza Sill. This allowed the overflow of the palaeo-MOW into the South Rifian Corridor, supporting the interpretation of the South Rifian Corridor having been subject to a palaeo-MOW, enabling the formation of a contourite depositional system like that described in the Gulf of Cadiz (Llave *et al.*, 2007; Hernández-Molina *et al.*, 2016).

The proposed facies model

De Castro *et al.* (2020b) proposed the first inclusive contourite facies model for contourite channel systems to date. This facies model has been constructed based on a multiple core related dataset derived from the Gulf of Cadiz. However, the core material does not cover most of the sand-rich intervals related to the contourite channel. Despite not fully capturing the contourite channel deposits, the proposed model shows many similarities but is distinctly more inclusive of the coarse-grained channel deposits (Fig. 12). Since currently no other facies models for contourite channel deposits have been proposed, results from this study cannot be compared any further.

The most challenging aspect of interpreting the deposits of facies association FA4 (contourite channel deposits) as having a contouritic origin arises from the tidal signatures observed (Fig. 10). The tidal signatures however can be explained by the tidal modulation of the palaeo-MOW as has been observed in the present-day MOW in the Strait of Gibraltar (Candela *et al.*, 1990).

Tidal modulation of the palaeo-Mediterranean Outflow Water

The late Miocene Taza Strait in the South Rifian Corridor shows many similarities to the closely located modern Strait of Gibraltar (SoG) such as the Atlantic–Mediterranean connection,

geometry, water-depths of a similar range and the presence of a sill (Camarinal Sill and Taza Sill, respectively) located in the narrowest position of the strait. Due to these similarities, flow variability through the South Rifian Corridor is expected to have behaved in a similar general fashion as the modern SoG. The flow variability through the modern SoG is herein discussed to explain the tidal signatures recognized in the Miocene Rifian deposits (i.e. cyclically thickening and thinning foresets, cyclic alterations between angular and tangential toe-set geometries and sand–mud couplets observed in facies F5, F6 and F7; Fig. 10).

Lacombe & Richez (1982) categorized flow variability through the SoG into three distinct types: long-term, subinertial and tidal. The long-term flow variability relates to the double layer baroclinic exchange between the Atlantic and Mediterranean basins. The exchange, or circulation, consists of Atlantic waters flowing into the Mediterranean overriding the denser Mediterranean Outflow Water flowing westward into the Atlantic (Armi & Farmer, 1988; Fig. 1B). This long-term flow variability is controlled by seasonal and interannual fluctuations in the evaporation–precipitation budget over the Mediterranean Sea, affecting Mediterranean Deep Water formation. The two-layer exchange is interpreted to be hydraulically controlled at the Camarinal and Spartel sills (intensification of the MOW) on the western half and at the Tarifa narrow (intensification of the Atlantic inflow) on the eastern side of the strait (Bryden & Stommel, 1984; Armi & Farmer, 1988). The subinertial or interannual mostly barotropic flow variability, with periods ranging from days to months, is forced by the atmospheric pressure field over the Mediterranean (Candela *et al.*, 1989; García Lafuente *et al.*, 2002). Tidal flows through the SoG are principally driven by the North Atlantic semidiurnal tide. Semidiurnal tides within the strait reach large amplitudes relative to subinertial flows, thus forming the dominant factor in flow variability (Candela *et al.*, 1990) and strongly modulating the long-term seasonal and interannual exchange pattern. On shorter, sub-daily timescales, modifications due to internal waves occur (Richez, 1994; Vázquez *et al.*, 2008).

As indicated by Rocha & Clarke (1987), the tidal wave arriving at a very narrow strait with a central sill is predominantly reflected, creating a standing tidal wave inside the strait. This standing wave, whose existence has been experimentally confirmed for the SoG (Candela *et al.*, 1990), generates barotropic tidal current peaks between high tide and low tide (Fig. 13B; ebb phase). The same authors indicated that due to the requirement of geostrophic adjustment in the across-strait direction maximum westward tidal currents are present between low tide and high tide (Fig. 13D; flood phase), diminishing the inflow of Atlantic water and intensifying the MOW. A maximum eastward tidal current is found in the ebb phase (Fig. 13B; between high tide and low tide), favouring Atlantic water inflow and diminishing or occasionally reversing the direction of the MOW. Both at high tide and low tide, the tidal current is zero, therefore, at both moments in the tidal cycle the MOW should approach its mean intensity (Fig. 13A and C).

Based on the analogies between the SoG and the Taza Strait it can be expected that during the late Miocene the Taza Strait was subjected to a similar hydrodynamic behaviour responsible for the tidally modulated, pulsating behaviour of the palaeo-MOW (Fig. 13E), recorded in the sedimentary successions of the El Adergha and Fes-north sections (Fig. 10). Because the MOW/palaeo-MOW forms/formed a bottom current which is/was the dominant process responsible for the redistribution and deposition of sediment, hydraulically modulated by tides, its deposits are considered contourites.

The signature of cyclic deceleration (ebb phase) and acceleration (flood phase) of the palaeo-MOW is recognized in FA4 (Fig. 10). These facies are associated with the contourite channel, the contourite element which is influenced most severely by hydrodynamic changes in the palaeo-MOW. Differences in the tidal signature between F5, F6 and F7 might be related to their position within the contourite channel. However, changes in the geometry and physiography of the strait margins (due to, for example, relative sea-level variations) and changes in water mass properties could potentially affect the tidal hydrodynamics of the palaeo-MOW as well.

The geometry of straits mainly controls the amplification of the tidal wave and the ability to transport water from one basin to another (Rocha & Clarke, 1987; Candela *et al.*, 1990). However, the Taza Strait is not expected to have changed geometry significantly over the period in which the sediments studied herein were deposited (7.35 to 7.25 Ma) as the main tectonic compressional event in the Rifian corridors took place around 7 Ma (Capella *et al.*,

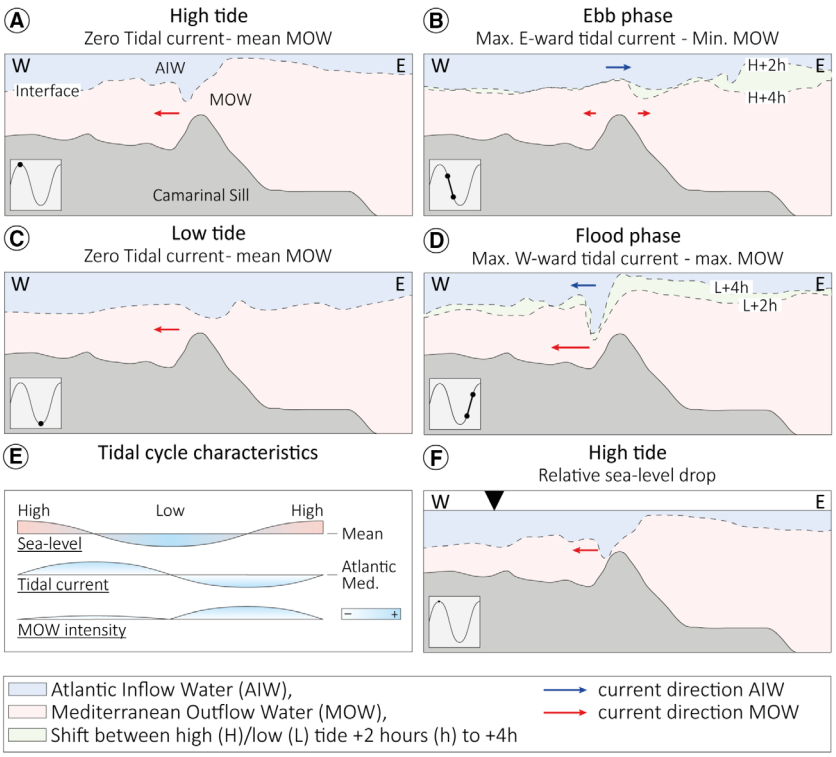

Fig. 13. (A) to (D) Influence of a tidal cycle on Atlantic Inflow Water (AIW) and Mediterranean Outflow Water (MOW) and the interface between the two. At high tide and low tide – (A) and (C), respectively – the tidal current is zero and the MOW reaches its mean intensity. During the ebb phase [from high tide to low tide (B)] the tidal current is directed towards the east and the MOW reaches its lowest velocity. Occasionally, the direction of the MOW can also be reversed. During the flood phase [from low tide to high tide (D)] the tidal current is directed towards the west and the MOW reaches its highest velocity. (E) Summarizes the water mass characteristics during one tidal cycle. (F) Shows the long-term effect of a relative sea-level drop, by which the interface is located closer to the sill. The location of the interface to the sill affects the potential of Mediterranean Deep Water (MDW) to flow out of the Mediterranean.

2017b; Tulbure *et al.*, 2017). Mud drapes and heterolithic muddy and sandy beds are an indicator for significant changes in hydrodynamic conditions, bedload transport and suspension fallout. Such changes recorded on foreset-scale and laminae-scale suggest significant tidally induced fluctuations between 'slack' water and bottom currents with velocities up to 1 m s^{-1}.

The strength of the MOW is mainly a result of the density differences between the overriding Atlantic inflow water and the underlying MOW (Rogerson *et al.*, 2012; Sierro *et al.*, 2020). If the density difference between the two water masses is higher, a stronger MOW is expected because of an increased effect of acceleration due to gravity. Tidal effects on the MOW should also be significantly affected by the average depth of the Atlantic–Mediterranean water interface with respect to the sill. If the interface is closer to the sill (Fig. 13F) tidal effects on the MOW should be amplified, generating larger differences between flood and ebb phases. As overflow requires a minimum depth to the sill (de la Vara *et al.* (2015), at times, when the interface is near the sill, the MOW might have even completely stopped as the interface reached the Atlantic side of the sill during the ebb phase. Processes that would result in an interface close to the sill are likely related to relative sea-level changes. Miller *et al.* (2011) reported however that because of the development of a near-permanent East Antarctic Ice Sheet, the middle Miocene to early Pliocene glacio-eustatic sea-level changes were muted. This, however, does not mean that relative sea-level changes in the order of tens of metres would have had a profound effect on the interface–sill characteristics.

Here, it is assumed that during the deposition of facies F7, consisting of sigmoidal mud-draped

sandstone, the Atlantic–Mediterranean interface was located close to the sill. This is explained by the strong tidally induced cyclic acceleration and deceleration changes inferred from the studied facies. Facies F6, consisting of cross-stratified sandstones lacking any mud, is expected to have been deposited when the interface was located well above the sill, decreasing tidal amplification. However, the thick foresets and relatively coarse grain sizes suggest that density differences between the Atlantic and Mediterranean were enhanced, allowing high velocity bottom currents. Facies F5, consisting of heterolithic cross-stratified mudstone and sandstone, is interpreted as an intermediate facies with relatively strong tidal fluctuations but lower-maximum current velocities.

Evolution of the contourite channel system

The vertical sedimentary facies stacking patterns observed in the Fes-north and El Adergha sections suggest that, over time, the depositional processes changed at the site where the sections were located. The comparison and correlation between the two sections is used to explain the lateral migration of the contourite depositional system and the intermittent flow of the palaeo-MOW. As the Fes-north section is located northwestward of the El Adergha section, it is assumed that it was located up-slope and down-current with respect to the westward flow-direction of the palaeo-MOW (Fig. 11). Since the down-current facies changes cannot be deduced from the vertical stacking of facies, this aspect will not be considered in the reconstruction of the system evolution. The relative distance between both sections has been considered constant over time. Based on the stratigraphic and facies (based on the proposed facies model) correlation, four main evolutionary phases have been identified (Fig. 14).

Phase 1 – The initiation or intensification of the palaeo-MOW related to a change from dominantly fine-grained deposits (FA1) to coarser grained deposits associated with FA3 and FA2 for the Fes-north and El Adergha sections, respectively (Fig. 14A and B). The initiation of an active palaeo-MOW in the study area is associated with the uplift of the accretionary wedge and the Prerifian Ridges. This tectonically driven event terminated the palaeo-MOW pathway north of these ridges that was active between 7.8 Ma and 7.51 Ma (de Weger *et al.*, 2020). As the palaeo-MOW was forced southward of the Prerifian Ridges this allowed the intensification of bottom current in this region. Over time this palaeo-MOW formed a contourite channel system in which the Fes-north section constituted the contourite channel and the El Adergha section the transitional channel-drift domain.

Phase 2 – The northward migration of the contourite depositional system is related to facies stacking patterns that suggest decreasing flow-velocities. These decreasing flow velocities are associated with a northward shift of the contourite depositional system where, in El Adergha, the depositional setting changes from drift-channel transition to drift, and in Fes-north, the depositional setting changes from channel to channel-flank or slope deposits (Fig. 14C to E). As the palaeo-MOW is forced northward by the Coriolis force, the system naturally migrates up-slope or northward (Faugères *et al.*, 1999; Llave *et al.*, 2001). This migration is stimulated by active erosion on the right (up-slope) flank of the channel and highest rates of deposition over the left flank, the drift. However, since channel facies overlie drift transitional facies (FA2) in the Fes-north section, FA2 in this section might be, although highly speculative, related to up-slope overbank deposits. These overbank deposits could be drift deposits associated with another water mass as similar features have been identified along the middle and upper slope of the Gulf of Cadiz at the exit of the SoG (Brackenridge *et al.*, 2018; García *et al.*, 2020). In the SoG these deposits are related to a different, shallower water mass compared to that of the contourite channel (García *et al.*, 2020).

Phase 3 – Reduction of the palaeo-MOW intensity is indicated by the disappearance of contourite facies related to high-velocity bottom currents. This allowed the preservation of turbidites (F8) in Fes-north and the deposition of fine-grained contourites or hemipelagites (FA1) in El Adergha (Fig. 14F and G). In the facies stacking pattern of this interval in El Adergha, minor fluctuations related to flow velocities have been observed, suggesting the intermittent behaviour of the palaeo-MOW. The reduction of the palaeo-MOW intensity is most likely associated with a decrease in the density gradient between Atlantic inflow and Mediterranean outflow water (Rogerson *et al.*, 2012). This decrease in density could be related to subduction of the Taza Strait, enabling increased inflow of less-saline Atlantic water, and reducing the formation of Mediterranean Deep Water. Since no evidence was found of eastward flow related to the inflow of Atlantic water, the

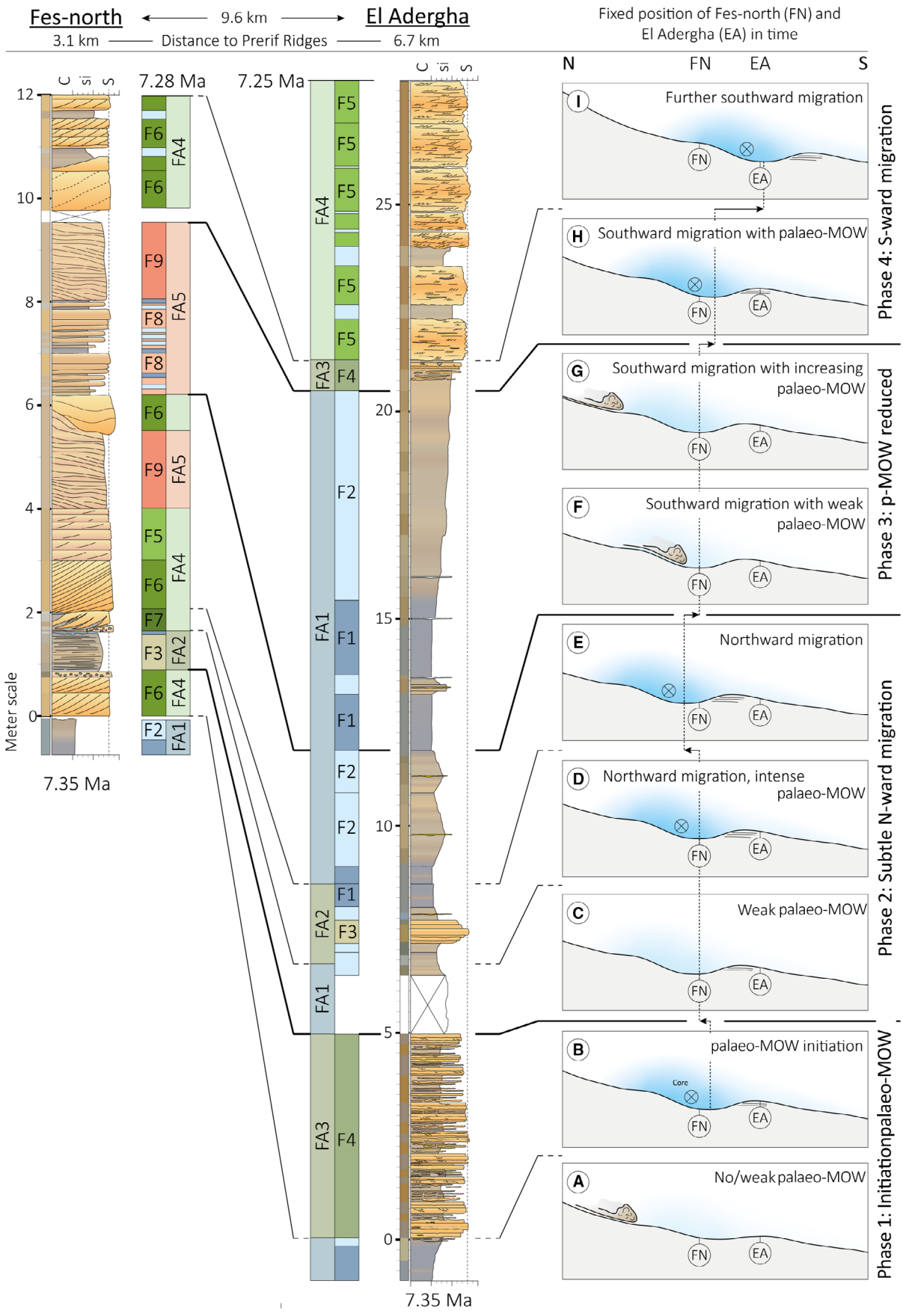

Fig. 14. The logs of the late Miocene Fes-north (FN) and El Adergha (EA) sections show vertical sedimentary facies changes. The vertical stacking of facies has been correlated based on their depositional ages (7.51 to 7.25 Ma) as well as on facies which, based on the herein proposed facies model, can be correlated in an across contourite channel system profile. (A) Depicts the transition from blue marls to more sand-rich marls which might indicate the initiation of a palaeo-Mediterranean Outflow Water (p-MOW) in the area. (B) Shows the clear transition from FA1 to facies related to bottom current processes. By this time, the palaeo-MOW became the dominant depositional process. (C) to (E) Depicts the subtle northward migration of the contourite depositional system (CDS) and a possible intensification of the palaeo-MOW. (F) and (G) Depicts a period with low-velocity bottom currents associated with a weak palaeo-MOW. During this period, gravitational deposits could be preserved, as they were not being significantly affected by bottom currents. (H) and (I) Depicts the southward migration of the CDS, where the channel (FA4) migrated of the drift (FA1).

palaeo-MOW was likely still present. This stratigraphic interval being dominated by gravitational deposits furthermore suggests that the slope was tectonically unstable. This tectonic instability was a precursor to the tectonically induced southward migration of the system as indicated in Phase 4.

The final phase – *Phase 4* – is marked by a significant southward migration of the contourite depositional system (Fig. 14H and I). This southward shift is recognized by the emplacement of contourite channel facies (FA4) over the drift facies (FA1) in El Adergha. The southward migration of the contourite channel system could be related to intensification of the density gradient between the Atlantic and the palaeo-MOW, supporting a deeper settling depth of the palaeo-MOW. Rogerson *et al.* (2012) however suggest that the negative feedback process of enhanced ambient water entrainment with a denser palaeo-MOW plume counteracts deeper settlement of this plume. As such, it is more likely that the palaeo-MOW was forced southward by tectonic uplift resulting in the southward migration of the contourite channel. Ongoing tectonic uplift since 7.25 Ma closed the Atlantic–Mediterranean connection leading to the Mediterranean Salinity Crisis (Capella *et al.*, 2020b).

Implications

The main controls on depositional style of contourite features are flow-velocity and the characteristics of sediment availability. Taking this into account, the resulting morphology and depositional style should not be drastically different between the studied sections and other contourite systems. Current velocities generated by overflow are however high in comparison to thermohaline circulation. Accordingly, the ability of the flow to transport and deposit sandy sediment is a function of flow-velocity and sediment particle characteristics [for example, the Hjulström curve (Hjulstrom, 1935)], and thus sandy contourite deposits independent of the style of bottom current generation should show similar features. As such, the contourite channel system and the erosional and depositional features are unique due to the morphology of the gateway and the effects of this morphology on flow characteristics. The gateway however was sufficiently wide (*ca* 30 km) not to restrict the palaeo-MOW, allowing it to 'freely' flow along the slope, controlled only by seafloor morphology, density gradients and the Coriolis force. The morphology of the gateway however amplified tidal forces generating a tidal control on overflow behaviour. Accordingly, it can be deduced that other contourite systems characterized by similar flow-velocities and not related to gateway systems, should likely show less pronounced tidal signatures.

CONCLUSIONS

The main findings described and discussed in this manuscript relate to the discovery and description of sandy contourites and their first ever recognition as being relics of a contourite channel system, cropping out in the ancient record. As such, they represent a valuable analogue for modern contourite depositional systems and ancient subsurface exploration and research targets.

The findings presented herein elaborate on the evolution of this system and emphasize the occurrence of different facies associated with bottom currents. Facies and facies associations have been interpreted as representing the 'full-spectrum' of contourite depositional and erosional environments, the drift, drift-channel transition and the contourite channel. The facies changes are predominantly related to

changes in the intensity of the palaeo-Mediterranean Outflow Water (palaeo-MOW) which decreases away from its core. The contourites are interstratified with hemipelagites, turbidites and slump deposits where their preservation is related to a decrease in palaeo-MOW intensity.

The vertical sedimentary facies stacking pattern records the tectonically induced, southward migration of the contourite depositional system (CDS) and the intermittent behaviour of the palaeo-MOW which is mainly driven by precessional-scale and millennial-scale climate variations. The tidal signature in the sandy contourite deposits shows that tides played a key factor in modulating the palaeo-MOW on a sub-annual timescale.

The results of this study indicate that bottom currents, their hydrodynamic conditions and their effect on deep-marine depositional processes and environments are controlled by: (i) the intermittent behaviour of flow (on–off); (ii) flow acceleration and deceleration; and (iii) tidal modulation. All of these factors should be considered in the process-based interpretation of all deep marine deposits possibly affected by bottom currents.

Keeping in mind, the well-known expression of 'the past is the key to the future', contourite research, such as this study, could significantly contribute to the understanding of processes leading to changes in global ocean circulation and associated climate change. As this manuscript provides information regarding mechanisms that affect the overflow of dense Mediterranean water and gateway evolution, which impacts global ocean circulation, this work provides information on processes that contribute to climate change.

ACKNOWLEDGEMENTS

We are very appreciative of the help and support given by the Office National des Hydrocarbures et des Mines (ONHYM), Morocco. This project was funded by the Joint Industry Project supported by TOTAL, BP, ENI, ExxonMobil, Wintershal DEA, and TGS, executed in the framework of "The Drifters Research Group" at Royal Holloway University of London (RHUL), related to projects CTM 2012039599-C03, CGL2016-80445-R and CTM2016-75129-C3-1-R. The research contribution of O. Salas-Miguez was funded through a pre-doctoral grant from the Ministerio de Educacion, Cultura y Deporte (Gobierno Espana). Journal reviews by A.R. Viana and S.G. Longhitano are greatly appreciated, and their comments helped us to improve the clarity of the manuscript.

DATA AVAILABILITY STATEMENT

The data that support the findings of this study are available from the corresponding author upon reasonable request.

REFERENCES

Achalhi, M., **Münch, P.**, **Cornée, J.J.**, **Azdimousa, A.**, **Melinte-Dobrinescu, M.**, **Quillévéré, F.**, **Drinia, H.**, **Fauquette, S.**, **Jiménez-Moreno, G.**, **Merzeraud, G.**, **Moussa, A.B.**, **El Kharim, Y.** and **Feddi, N.** (2016) The late Miocene Mediterranean-Atlantic connections through the north Rifian corridor: new insights from the Boudinar and Arbaa Taourirt basins (northeastern Rif, Morocco). *Palaeogeogr. Palaeoclimatol. Palaeoecol.*, **459**, 131–152.

Allen, J.R.L. (1982) Mud drapes in sand-wave deposits: a physical model with application to the Folkestone Beds (early Cretaceous, southeast England). *Phil. Trans. Roy. Soc. London. Series A. Math. Phys. Sci.*, **306**, 291–345.

Armi, L. and **Farmer, D.M.** (1988) The flow of Mediterranean water through the Strait of Gibraltar. *Prog. Oceanogr.*, **21**, 1–105.

Barbero, L., **Jabaloy, A.**, **Gómez-Ortiz, D.**, **Pérez-Peña, J.V.**, **Rodríguez-Peces, M.J.**, **Tejero, R.**, **Estupiñán, J.**, **Azdimousa, A.**, **Vázquez, M.** and **Asebriy, L.** (2011) Evidence for surface uplift of the Atlas Mountains and the surrounding peripheral plateaux: Combining apatite fission-track results and geomorphic indicators in the Western Moroccan Meseta (coastal Variscan Paleozoic basement). *Tectonophysics*, **502**, 90–104.

Barbieri, R. and **Ori, G.G.** (2000) Neogene palaeoenvironmental evolution in the Atlantic side of the Rifian Corridor (Morocco). *Palaeogeogr. Palaeoclimatol. Palaeoecol.*, **163**, 1–31.

Barhoun, N. and **Taoufio, N.B.** (2008) Biostratigraphic and environmental events recorded in the Riffian southern corridor (Northern Morocco) in late Miocene before the Messinian salinity crisis. *Geodiversitas*, **30**, 21–40.

Bernini, M., **Boccaletti, M.**, **El Mokhtari, J.**, **Gelati, R.**, **Iaccarino, S.**, **Moratti, G.** and **Papani, G.** (1992) Données stratigraphiques nouvelles sur le Miocène supérieur du bassin de Taza-Guercif (Maroc nord- oriental). *Bulletin de la Société géologique de France*, **163**, 73–76.

Betzler, C., **Braga, J.C.**, **Martín, J.M.**, **Sanchez-Almazo, I.M.** and **Lindhorst, S.** (2006) Closure of a seaway: stratigraphic record and facies (Guadix basin, Southern Spain). *Int. J. Earth Sci.*, **95**, 903–910.

Bouma, A.H. (1962) Sedimentology of some flysch deposits. *A graphic approach to facies interpretation*, pp. 168.

Brackenridge, R.E., **Stow, D.A.V.**, **Hernández-Molina, F.J.**, **Jones, C.**, **Mena, A.**, **Alejo, I.**, **Ducassou, E.**, **Llave, E.**, **Ercilla, G.**, **Nombela, M.A.**, **Perez-Arlucea, M.** and

Frances, G. (2018) Textural characteristics and facies of sand-rich contourite depositional systems. *Sedimentology*, **65**, 2223–2252. https://doi.org/10.1111/sed.12463.

Bryden, H.L. and **Stommel, H.M.** (1984) Limiting processes that determine basic features of the circulation in the Mediterranean Sea. *Oceanol. Acta*, **7**, 289–296.

Buatois, L.A. and **Mángano, M.G.** (2011) *Ichnology: Organism-substrate Interactions in Space and Time*. Cambridge University Press, Cambridge, 358 pp.

Candela, J. (2001) Mediterranean water and global circulation. *Int. Geophys, Academic Press.*, **77**, 419-XLVIII.

Candela, J., **Winant, C.D.** and **Ruiz, A.** (1989) Meteorologically forced subinertial flows through the Strait of Gibraltar. *J. Geogphys. Res.*, **94**, 12667–12674.

Candela, J., **Winant, C.** and **Ruiz, A.** (1990) Tides in the Strait of Gibraltar. *J. Geophys. Res.*, **95**, 7313–7335.

Capella, W., **Barhoun, N.**, **Flecker, R.**, **Hilgen, F.J.**, **Kouwenhoven, T.**, **Matenco, L.C.**, **Sierro, F.J.**, **Tulbure, M.A.**, **Yousfi, M.Z.** and **Krijgsman, W.** (2018) Palaeogeographic evolution of the late Miocene Rifian Corridor (Morocco): reconstructions from surface and subsurface data. *Earth Sci Rev*, **180**, 37–59.

Capella, W., **Hernández-Molina, F.j.**, **Flecker, R.**, **Hilgen, F.j.**, **Hssain, M.**, **Kouwenhoven, T.j.**, **van Oorschot, M.**, **Sierro, F.j.**, **Stow, D.**, **Trabucho-Alexandre, J.**, **Tulbure, M.a.**, **de Weger, W.**, **Yousfi, M.z.** and **Krijgsman, W.** (2017a) Sandy contourite drift in the late Miocene Rifian Corridor (Morocco): Reconstruction of depositional environments in a foreland-basin seaway. *Sed. Geol.*, **355**, 31–57.

Capella, W., **Matenco, L.**, **Dmitrieva, E.**, **Roest, W.M.**, **Hessels, S.**, **Hssain, M.**, **Chakor-Alami, A.**, **Sierro, F.J.** and **Krijgsman, W.** (2017b) Thick-skinned tectonics closing the Rifian Corridor. *Tectonophysics*, **710**, 249–265.

de Castro, S., **Hernández-Molina, F.J.**, **Rodríguez-Tovar, F.J.**, **Llave, E.**, **Ng, Z.L.**, **Nishida, N.** and **Mena, A.** (2020a) Contourites and bottom current reworked sands: Bed facies model and implications. *Mar. Geol.*, **428**, 106267.

de Castro, S., **Hernández-Molina, F.J.**, **de Weger, W.**, **Jiménez-Espejo, F.J.**, **Rodriguez-Tovar, F.J.**, **Mena, A.**, **Llave, E.** and **Sierro, F.J.** (2020b) Contourite characterisation and its discrimination from other deep-water deposits in the Gulf of Cadiz contourite depositional system. *Sedimentology*, https://doi.org/10.1111/sed.12813

de Castro, S., **Miramontes, E.**, **Dorador, J.**, **Jouet, G.**, **Cattaneo, A.**, **Rodríguez-Tovar, F.J.** and **Hernández-Molina, F.J.** (2021) Siliciclastic and bioclastic contouritic sands: Textural and geochemical characterisation. *Marine Petrol. Geol.*, **128**, 105002.

Chalouan, A. and **Michard, A.** (2004) The Alpine Rif Belt (Morocco): a case of mountain building in a subduction-subduction-transform fault triple junction. *Pure Appl Geophys*, **161**, 489–519.

Chen, Y., **Yao, G.**, **Wang, X.**, **Lv, F.**, **Shao, D.**, **Lu, Y.**, **Cao, Q.** and **Tang, P.** (2020) Flow processes of the interaction between turbidity flows and bottom currents in sinuous unidirectionally migrating channels: An example from the Oligocene channels in the Rovuma Basin, offshore Mozambique. *Sediment. Geol.*, **404**, 105680.

Chiarella, D. (2016) Angular and tangential toeset geometry in tidal cross-strata: An additional feature of current-modulated deposits. In: *Contributions to Modern and Ancient Tidal Sedimentology: Proceedings of the Tidalites 2012 Conference* (Eds Tessier, B. and Reynaud, J.Y.), 1st edn, pp. 191–201. John Wiley & Sons, Ltd, Hoboken.

Chiarella, D., **Longhitano, S.G.** and **Tropeano, M.** (2017) Types of mixing and heterogeneities in siliciclastic-carbonate sediments. *Mar. Petrol. Geol.*, **88**, 617–627.

Corbí, H., **Lancis, C.**, **García-García, F.**, **Pina, J.A.**, **Soria, J.M.**, **Tent-Manclús, J.E.** and **Viseras, C.** (2012) Updating the marine biostratigraphy of the Granada Basin (central Betic Cordillera). Insight for the Late Miocene palaeogeographic evolution of the Atlantic-Mediterranean seaway. *Geobios*, **45**, 249–263.

Creaser, A., **Hernández-Molina, F.J.**, **Badalini, G.**, **Thompson, P.**, **Walker, R.**, **Soto, M.** and **Conti, B.** (2017) A Late Cretaceous mixed (turbidite-contourite) system along the Uruguayan Margin: Sedimentary and palaeoceanographic implications. *Mar. Geol.*, **390**, 234–253.

De La Vara, A., **Topper, R.P.**, **Meijer, P.T.** and **Kouwenhoven, T.J.** (2015) Water exchange through the Betic and Rifian corridors prior to the Messinian Salinity Crisis: A model study. *Paleoceanography*, **30**, 548–557.

DiGeronimo, I., **Grasso, M.** and **Pedley, H.M.** (1981) Palaeoenvironment and palaeogeography of Miocene marls from Southeast Sicily and the Maltese Islands. *Palaeogeogr. Palaeoclimatol. Palaeoecol.*, **34**, 173–189.

Einsele, G. (2000) *Sedimentary Basins: Evolution, Facies, and Sediment Budget*. Springer Science & Business Media, Berlin.

Faas, R.W. (1991) Rheological boundaries of mud: where are the limits? *Geo-Mar. Lett.*, **11**, 143–146.

Faugères, J.C., **Gonthier, E.** and **Stow, D.A.V.** (1984) Contourite drift molded by deep Mediterranean outflow. *Geology*, **12**, 296–300.

Faugères, J.C., **Stow, D.A.V.**, **Imbert, P.** and **Viana, A.** (1999) Seismic features diagnostic of contourite drifts. *Mar. Geol.*, **162**, 1–38.

Feinberg, H. (1986) Les séries tertiaires des zones externes du Rif (Maroc): biostratigraphie, paléogéographie et aperçu tectonique. Éditions du Service géologique du Maroc, (No. 315).

Flecker, R., **Krijgsman, W.**, **Capella, W.**, **de Castro Martíns, C.**, **Dmitrieva, E.**, **Mayser, J.P.**, **Marzocchi, A.**, **Modestou, S.**, **Ochoa, D.**, **Simon, D.**, **Tulbure, M.**, **van den Berg, B.**, **van der Schee, M.**, **de Lange, G.**, **Ellam, R.**, **Govers, R.**, **Gutjahr, M.**, **Hilgen, F.**, **Kouwenhoven, T.**, **Lofi, J.**, **Meijer, P.**, **Sierro, F.J.**, **Bachiri, N.**, **Barhoun, N.**, **Alami, A.C.**, **Chacon, B.**, **Flores, J.A.**, **Gregory, J.**, **Howard, J.**, **Lunt, D.**, **Ochoa, M.**, **Pancost, R.**, **Vincent, S.** and **Yousfi, M.Z.** (2015) Evolution of the Late Miocene Mediterranean-Atlantic gateways and their impact on regional and global environmental change. *Earth-Sci. Rev.*, **150**, 365–392.

Flinch, J. (1993) *Tectonic evolution of the Gibraltar arc* [Ph. D. thesis]. Rice University, Houston, TX.

Fonnesu, M., **Palermo, D.**, **Galbiati, M.**, **Marchesini, M.**, **Bonamini, E.** and **Bendias, D.** (2020) A new world-class deep-water play-type, deposited by the syndepositional interaction of turbidity flows and bottom currents: The giant Eocene Coral Field in northern Mozambique. *Mar. and Petrol. Geol.*, **111**, 179–201.

Fuhrmann, A., **Kane, I.A.**, **Clare, M.A.**, **Ferguson, R.A.**, **Schomacker, E.**, **Bonamini, E.** and **Contreras, F.A.** (2020) Hybrid turbidite-drift channel complexes: An integrated multiscale model. *Geology*, **48**, 562–568.

García Lafuente, J., **Álvarez, E.**, **Vargas, J.M.** and **Ratsimandresey, W.** (2002) Subinertial variability in the flow through the Strait of Gibraltar. *J. of Geophys. Res.*, **107**, 32.1–32.9.

García, M., **Llave, E.**, **Hernández-Molina, F.J.**, **Lobo, F.J.**, **Ercilla, G.**, **Alonso, B.**, **Casas, D.**, **Mena, A.** and **Fernández-Salas, L.M.** (2020) The role of late Quaternary tectonic activity and sea-level changes on sedimentary processes interaction in the Gulf of Cadiz upper and middle continental slope (SW Iberia). *Mar. Petrol. Geol.*, **121**, 104595.

Gelati, R., **Moratti, G.** and **Papani, G.** (2000) The Late Cenozoic sedimentary succession of the Taza-Guercif Basin, South Rifian Corridor, Morocco. *Mar. Petrol. Geol.*, **17**, 373–390.

Gonthier, E.G., **Faugères, J.C.** and **Stow, D.A.V.** (1984) Contourite facies of the Faro drift, Gulf of Cadiz. *J. Geol. Soc. London, Special Publications*, **15**, 275–292.

Hernández-Molina, F.J., **Campbell, S.**, **Badalini, G.**, **Thompson, P.**, **Walker, R.**, **Soto, M.**, **Conti, B.**, **Preu, B.**, **Thieblemont, A.**, **Hyslop, L.**, **Miramontes, E.** and **Morales, E.** (2018) Large bedforms on contourite terraces: Sedimentary and conceptual implications. *Geology*, **46**, 27–30.

Hernández-Molina, F.J., **Llave, E.**, **Stow, D.A.V.**, **García, M.**, **Somoza, L.**, **Vázquez, J.T.**, **Lobo, F.J.**, **Maestro, A.**, **Diaz del Rio, V.**, **Leon, R.**, **Medialdea, T.** and **Gardner, J.** (2006) The contourite depositional system of the Gulf of Cadiz: a sedimentary model related to the bottom current activity of the Mediterranean outflow water and its interaction with the continental margin. *Deep Sea Res Part II*, **53**, 1420–1463.

Hernández-Molina, F.J., **Llave, E.** and **Stow, D.A.V.** (2008) Continental slope contourites. *Dev. Sedimentol.*, **60**, 379–408.

Hernández-Molina, F.J., **Llave, E.**, **Preu, B.**, **Ercilla, G.**, **Fontan, A.**, **Bruno, M.**, **Serra, N.**, **Gomiz, J.J.**, **Brackenridge, R.E.**, **Sierro, F.J.**, **Stow, D.A.V.**, **Garcia, M.**, **Juan, C.**, **Sandoval, N.** and **Mrnaliz, A.** (2014a) Contourite processes associated with the Mediterranean Outflow Water after its exit from the Strait of Gibraltar: Global and conceptual implications. *Geology*, **42**, 227–230.

Hernández-Molina, F.J., **Paterlini, M.**, **Violante, R.**, **Marshall, P.**, **de Isasi, M.**, **Somoza, L.** and **Rebesco, M.** (2009) Contourite depositional system on the Argentine Slope: An exceptional record of the influence of Antarctic water masses. *Geology*, **37**, 507–510.

Hernández-Molina, F.J., **Soto, M.**, **Piola, A.R.**, **Tomasini, J.**, **Preu, B.**, **Thompson, P.**, **Badalini, G.**, **Creaser, A.**, **Violante, R.A.**, **Morales, E.**, **Paterlini, M.** and **De Santa Ana, H.** (2016a) A contourite depositional system along the Uruguayan continental margin: sedimentary, oceanographic and paleoceanographic implications. *Mar. Geol.*, **378**, 333–349.

Hernández-Molina, F.J., **Stow, D.A.V.**, **Alvarez-Zarikian, C.A.**, **Acton, G.**, **Bahr, A.**, **Balestra, B.**, **Ducassou, E.**, **Flood, R.**, **Flores, J.A.**, **Furota, S.**, **Grunert, P.**, **Hodell, D.**, **Jimenez-Espejo, F.**, **Kim, J.K.**, **Krissek, L.**, **Kuroda, J.**, **Li, B.**, **Llave, E.**, **Lofi, J.**, **Lourens, L.**, **Miller, M.**, **Nanayama, F.**, **Nishida, N.**, **Richter, C.**, **Roque, C.**, **Pereira, H.**, **Sanchez Goñi, M.F.**, **Sierro, F.J.**, **Singh, A.D.**, **Sloss, C.**, **Takashimizu, Y.**, **Tzanova, A.**, **Voelker, A.H.L.**, **Williams, T.** and **Xuan, C.** (2014b) Onset of Mediterranean outflow into the North Atlantic. *Science*, **344**, 1244–1250.

Hernández-Molina, F.J., **Wåhlin, A.**, **Bruno, M.**, **Ercilla, G.**, **Llave, E.**, **Serra, N.**, **Roson, G.**, **Puig, P.**, **Rebesco, M.**, **Van Rooij, D.**, **Roque, D.**, **Gonzalez-Pola, C.**, **Sanchez, F.**, **Gomez, M.**, **Preu, B.**, **Schwenk, T.**, **Hanebuth, T.J.J.**, **Sanchez Leal, F.S.**, **Garcia-Lafuente, J.**, **Brackenridge, R.E.**, **Juan, C.**, **Stow, D.A.V.** and **Maria Sanchez-Gonzalez, J.M.** (2016b) Oceanographic processes and morphosedimentary products along the Iberian margins: A new multidisciplinary approach. *Mar. Geol.*, **378**, 127–156.

Hesse, R. (1975) Turbiditic and non-turbiditic mudstone of Cretaceous flysch sections of the East Alps and other basins. *Sedimentology*, **22**, 387–416.

Hilgen, F.J., **Bissoli, L.**, **Iaccarino, S.**, **Krijgsman, W.**, **Meijer, R.**, **Negri, A.** and **Villa, G.** (2000) Integrated stratigraphy and astrochronology of the Messinian GSSP at Oued Akrech (Atlantic Morocco). *Earth Planet. Sci. Lett.*, **182**, 237–251.

van Hinsbergen, D.J., **Vissers, R.L.** and **Spakman, W.** (2014) Origin and consequences of western Mediterranean subduction, rollback, and slab segmentation. *Tectonics*, **33**, 393–419.

Hjulstrom, F. (1935) Studies of the morphological activity of rivers as illustrated by the river fyris, bulletin. *Geol. Instit. Upsalsa*, **25**, 221–527.

Hovikoski, J., **Uchman, A.**, **Weibel, R.**, **Nøhr-Hansen, H.**, **Sheldon, E.**, **Ineson, J.**, **Bjerager, M.**, **Therkelsen, J.**, **Olivarius, M.**, **Larsen, M.**, **Alsen, P.** and **Bojesen-Koefoed, J.** (2020) Upper Cretaceous bottom current deposits, north-east Greenland. *Sedimentology*. https://doi.org/10.1111/sed.12764

Hsü, K.J., **Ryan, W.B.** and **Cita, M.B.** (1973) Late Miocene desiccation of the Mediterranean. *Nature*, **242**, 240–244.

Hüneke, H., **Hernandez-Molina, F.**, **Rodríguez-Tovar, F.**, **Llave, E.**, **Chiarella, D.**, **Mena, A.** and **Stow, D.** (2020) Diagnostic criteria using microfacies for calcareous contourites, turbidites and pelagites in the Eocene-Miocene slope succession, southern Cyprus. *Sedimentology*. https://doi.org/10.1111/sed.12792

Hüneke, H. and **Stow, D.A.V.** (2008) Identification of ancient contourites: problems and palaeoceanographic significance. *Dev. Sedimentol.*, **60**, 323–344.

Iribarren, L., **Vergés, J.** and **Fernàndez, M.** (2009) Sediment supply from the Betic-Rif orogen to basins through Neogene. *Tectonophysics*, **475**, 68–84.

Knaust, D. (2017) *Atlas of trace fossils in well core: appearance, taxonomy and interpretation*. Springer International, Cham, 209 pp.

Krijgsman, W., **Capella, W.**, **Simon, D.**, **Hilgen, F.J.**, **Kouwenhoven, T.J.**, **Meijer, P.T.**, **Sierro, F.J.**, **Tulbure, M.A.**, **van den Berg, C.**, **van der Schee, M.** and **Flecker, R.** (2018) The Gibraltar corridor: Watergate of the Messinian salinity crisis. *Mar. Geol.*, **403**, 238–246.

Krijgsman, W., **Garcés, M.**, **Agustı, J.**, **Raffi, I.**, **Taberner, C.** and **Zachariasse, W.J.** (2000) The 'Tortonian salinity crisis' of the eastern Betics (Spain). *Earth Planet Sci. Lett.*, **181**, 497–511.

Krijgsman, W., **Langereis, C.G.**, **Zachariasse, W.J.**, **Boccaletti, M.**, **Moratti, G.**, **Gelati, R.**, **Laccarino, S.**, **Papani, G.** and **Villa, G.** (1999) Late Neogene evolution of the Taza-Guercif Basin (Rifian Corridor, Morocco) and implications for the Messinian salinity crisis. *Mar. Geol.*, **153**, 147–160.

Krijgsman, W., **Leewis, M.E.**, **Garcés, M.**, **Kouwenhoven, T.J.**, **Kuiper, K.F.** and **Sierro, F.J.** (2006) Tectonic control for evaporite formation in the Eastern Betics (Tortonian; Spain). *Sed. Geol.*, **188**, 155–170.

Lacombe, H. and **Richez, C.** (1982) The regime of the Strait of Gibraltar. In: *Hydrodynamics of Semi-Enclosed Seas* (Ed. Nihoul, J.C.J.), pp. 13–73.Elsevier Sci. Publ. Comp, New York, NY.

Leeder, M.R. (2009) *Sedimentology and Sedimentary Basins: From Turbulence to Tectonics*. John Wiley & Sons, London, 784 pp.

Llave, E., **Hernández-Molina, F.J.**, **Somoza, L.**, **Díaz-del-Río, V.**, **Stow, D.A.V.**, **Maestro, A.** and **Dias, J.A.** (2001) Seismic stacking pattern of the Faro-Albufeira contourite system (Gulf of Cadiz): a Quaternary record of paleoceanographic and tectonic influences. *Mar. Geophys. Res.*, **22**, 487–508.

Llave, E., **Hernández-Molina, F.J.**, **Somoza, L.**, **Stow, D.A.V.** and **Del Río, V.D.** (2007) Quaternary evolution of the contourite depositional system in the Gulf of Cadiz. *Geol. Soc., London, Spec. Public.*, **276**, 49–79.

Longhitano, S.G., **Mellere, D.**, **Steel, R.J.** and **Ainsworth, R.B.** (2012) Tidal depositional systems in the rock record: a review and new insights. *Sed. Geol.*, **279**, 2–22.

Longhitano, S.G. and **Nemec, W.** (2005) Statistical analysis of bed-thickness variation in a Tortonian succession of biocalcarenitic tidal dunes, Amantea Basin, Calabria, southern Italy. *Sed. Geol.*, **179**, 195–224.

Lowe, D.R. (1982) Sediment gravity flows; II, Depositional models with special reference to the deposits of high-density turbidity currents. *J. Sed. Res.*, **52**, 279–297.

Lozano, P., **Fernández-Salas, L.M.**, **Hernández-Molina, F.J.**, **Sánchez-Leal, R.**, **Sánchez-Guillamón, O.**, **Palomino, D.**, **Farias, C.**, **Mateo-Ramírez, A.**, **López-González, N.**, **García, M.**, **Vázquez, J.T.**, **Vila, Y.** and **Rueda, J.L.** (2020) Multiprocess interaction shaping geoforms and controlling substrate types and benthic community distribution in the Gulf of Cádiz. *Mar. Geol.*, **423**, 106139.

Lucchi, R.G. and **Rebesco, M.** (2007) Glacial contourites on the Antarctic Peninsula margin: insight for palaeoenvironmental and palaeoclimatic conditions. *Geol. Soc. London Spec. Publ.*, **276**, 111–127.

MacEachern, J.A., **Bann, K.L.**, **Gingras, M.K.**, **Zonneveld, J.P.**, **Dashtgard, S.E.** and **Pemberton, S.G.** (2012) The ichnofacies paradigm. *Dev. Sedimentol.*, **64**, 103–138.

MacEachern, J.A., **Pemberton, S.G.**, **Gingras, M.K.** and **Bann, K.L.** (2007) The ichnofacies paradigm: a fifty-year retrospective. In: *Trace fossils*. pp. 52–77. Elsevier, Amsterdam.

Mansour, B. and **Saint-Martin, J.P.** (1999) Conditions de depôt des diatomites messiniennes en contexte de plateforme carbonatée d'après l'etude des assemblages de diatomées: Exemple du Djebel Murdjadjo (Algérie). *Geobios*, **32**, 395–408.

Martín, J.M., **Braga, J.C.** and **Betzler, C.** (2001) The Messinian Guadalhorce corridor: the last northern, Atlantic-Mediterranean gateway. *Terra Nova*, **13**, 418–424.

Martín-Chivelet, J., **Fregenal-Martínez, M.A.** and **Chacón, B.** (2008) Traction structures in contourites. *Dev. Sedimentol.*, **60**, 157–182.

McCave, I.N. and **Tucholke, B.E.** (1986) Deep current-controlled sedimentation in the western North Atlantic. *Geol. Soc. Am*, **M**, 451–468.

Michard, A., **Saddiqi, O.**, **Chalouan, A.**, **de Lamotte, D.F.** (Eds.) (2008) *Continental Evolution: The Geology of Morocco: Structure, Stratigraphy, and Tectonics of the Africa-Atlantic-Mediterranean Triple Junction*, Vol. **116**. Springer, Berlin; Heidelberg.

Miguez-Salas, O., **Rodríguez-Tovar, F.J.** and **de Weger, W.** (2020) Macaronichnus and contourite depositional settings: Bottom currents and nutrients as coupling factors. *Palaeogeogr. Palaeoclimatol. Palaeoecol.*, **545**, 109639.

Miller, K.G., **Mountain, G.S.**, **Wright, J.D.** and **Browning, J.V.** (2011) A 180- million-year record of sea level and ice volume variations from continental margin and deep-sea isotopic records. *Oceanography*, **24**, 40–53.

Millot, C. (1999) Circulation in the western Mediterranean Sea. *J. Mar. Syst.*, **20**, 423–442.

Mulder, T. (2011) Gravity processes and deposits on continental slope, rise and abyssal plains. *Dev.Sedimentol.*, **33**, 25–148.

Mutti, E. (1992) *Turbidite Sandstones*. AGIP, Istituto di geologia, Università di Parma, Parma.

Mutti, E., **Bernoulli, D.**, **Lucchi, F.R.** and **Tinterri, R.** (2009) Turbidites and turbidity currents from Alpine 'flysch' to the exploration of continental margins. *Sedimentology*, **56**, 267–318.

Mutti, E., **Cunha, R.S.**, **Bulhoes, E.M.**, **Arienti, L.M.** and **Viana, A.R.** (2014) Contourites and turbidites of the Brazilian marginal basins. *AAPG Search Discov. Article*, **51069**, 1–46.

Nelson, C.H., **Baraza, J.** and **Maldonado, A.** (1993) Mediterranean undercurrent sandy contourites, Gulf of Cadiz, Spain. *Sed. Geol.*, **82**, 103–131.

Nelson, C.H., **Baraza, J.**, **Maldonado, A.**, **Rodero, J.**, **Escutia, C.** and **Barber Jr, J.H.** (1999) Influence of the Atlantic inflow and Mediterranean outflow currents on Late Quaternary sedimentary facies of the Gulf of Cadiz continental margin. *Mar. Geol.*, **155**, 99–129.

Nio, S.D. and **Yang, C.S.** (1991) Diagnostic attributes of clastic tidal deposits: a review. Clastic Tidal Sedimentology - Memoir 16, 1991. Recognition Criteria and Facies Models, pp. 3–27. Available at: https://archives.datapages.com/data/cspg_sp/data/016/016001/3_cspgsp0160003.htm

O'Brien, N.R., **Nakazawa, K.** and **Tokuhashi, S.** (1980) Use of clay fabric to distinguish turbiditic and hemipelagic siltstones and silts. *Sedimentology*, **27**, 47–61. https://doi.org/10.1111/j.1365-3091.1980.tb01157.x

Paulat, M., **Lüdmann, T.**, **Betzler, C.** and **Eberli, G.P.** (2019) Neogene palaeoceanographic changes recorded in a carbonate contourite drift (Santaren Channel, Bahamas). *Sedimentology*, **66**, 1361–1385.

Pérez-Asensio, J.N., **Aguirre, J.**, **Schmiedl, G.** and **Civis, J.** (2012) Messinian paleoenvironmental evolution in the lower Guadalquivir Basin (SW Spain) based on benthic foraminifera. *Palaeogeogr. Palaeoclimatol. Palaeoecol.*, **326**, 135–151.

Reading, H.G. (Ed.) (2009) *Sedimentary Environments: Processes, Facies and Stratigraphy*. John Wiley & Sons, Oxford, 704 pp.

Rebesco, M., **Hernández-Molina, F.J.**, **Van Rooij, D.** and **Wåhlin, A.** (2014) Contourites and associated sediments controlled by deep-water circulation processes: state-of-the-art and future considerations. *Mar. Geol.*, **352**, 111–154.

Rebesco, M., **Pudsey, C.J.**, **Canals, M.**, **Camerlenghi, A.**, **Barker, P.F.**, **Estrada, F.** and **Giorgetti, A.** (2002) Sediment drifts and deep-sea channel systems, Antarctic Peninsula Pacific Margin. *Geol. Soc. London, Mem.*, **22**, 353–371.

Richez, C. (1994) Airborne synthetic aperture radar tracking of internalwaves in the Strait of Gibraltar. *Prog. Oceanogr.*, **33**, 93–159.

Rocha, C.A. and **Clarke, A.J.** (1987) Interaction of ocean tides through a narrow single strait and narrow multiple straits. *J. Phys. Oceanogr.*, **17**, 2203–2218.

Rodrigues, S., **Hernández-Molina, F.J.** and **Kirby, A.** (2021) A Late Cretaceous hybrid (turbidite-contourite) system along the Argentine Margin: Paleoceanographic and conceptual implications. *Mar. and Petrol. Geol.*, **123**, 104768.

Rodríguez-Tovar, F.J., **Hernández-Molina, F.J.**, **Hüneke, H.**, **Llave, E.** and **Stow, D.A.V.** (2019) Contourite facies model: Improving contourite characterization based on the ichnological analysis. *Sed. Geol.*, **384**, 60–69.

Rogerson, M., **Rohling, E.J.**, **Bigg, G.R.** and **Ramirez, J.** (2012) Paleoceanography of the Atlantic- Mediterranean exchange: Overview and first quantitative assessment of climatic forcing. *Rev. Geophys.*, **50**, RG2003.

Rohling, E.J., **Marino, G.** and **Grant, K.M.** (2015) Mediterranean climate and oceanography, and the periodic development of anoxic events (sapropels). *Earth Sci. Rev.*, **143**, 62–97.

Roldán, F.J., **Galindo-Zaldívar, J.**, **Ruano, P.**, **Chalouan, A.**, **Pedrera, A.**, **Ahmamou, M.**, **Ruiz-Constan, A.**, **Sanz de Galdeano, C.**, **Benmakhlouf, M.**, **Lopez-Garrido, A.C.**, **Anahnah, F.** and **Gonzalez-Castillo, L.** (2014) Basin evolution associated to curved thrusts: The Prerifian Ridges in the Volubilis area (Rif Cordillera, Morocco). *J. Geodynamics*, **77**, 56–69.

Ryan, W.B.F. and **Hsü, K.J.** (1973*) Initial Reports of the Deep-Sea Drilling Project, 13*. US Govt. Printing Office, Washington, DC.

Saadi, S.E.M., **Hiladi, E.A.** and **Boudda, A.** (1980) *Notes et Memoires N°. Maquette achevée en (1975)*. Editions du Service Géologique du Maroc, Rabat.

Sani, F., **Del Ventisette, C.**, **Montanari, D.**, **Bendkik, A.** and **Chenakeb, M.** (2007) Structural evolution of the Rides Prerifaines (Morocco): structural and seismic interpretation and analogue modelling experiments. *Int. J. Earth Sci.*, **96**, 685–706.

Sansom, P. (2018) Hybrid turbidite–contourite systems of the Tanzanian margin. *Petrol. Geosci.*, **24**, 258–276.

Shanmugam, G. (2008) Deep-water bottom currents and their deposits. *Dev. Sedimentol.*, **60**, 59–81.

Shanmugam, G. (2010) Slides, slumps, debris flow, and turbidity currents. *Ocean Curr. Derivat. Encycl. Ocean Sci.*, **20**, 418.

Shanmugam, G. (2017) The contourite problem. In: *Sediment Provenance*, pp. 183–254. Elsevier, Amsterdam.

Shanmugam, G. (2020) *Mass Transport, Gravity Flows, and Bottom Currents: Downslope and Alongslope Processes and Deposits*. Elsevier, Amsterdam, 608 pp.

Sierro, F.J. (1985) The replacement of the "Globorotalia menardii" group by the Globorotalia miotumida group: An aid to recognizing the Tortonian-Messinian boundary in the Mediterranean and adjacent Atlantic. *Mar. Micropaleontol.*, **9**, 525–535.

Sierro, F.J., **Flores, J.A.**, **Civis, J.**, **Gonza, J.A.** and **France, G.** (1993) Late Miocene globorotaliid event- stratigraphy and biogeography in the NE-Atlantic and Mediterranean. *Mar. Micropaleontol.*, **21**, 143–167.

Sierro, F.J., **Hilgen, F.J.**, **Krijgsman, W.** and **Flores, J.A.** (2001) The Abad composite (SE Spain): a Messinian reference section for the Mediterranean and the APTS. *Palaeogeogr. Palaeoclimatol. Palaeoecol.*, **168**, 141–169.

Sierro, F.J., **Hodell, D.A.**, **Andersen, N.**, **Azibeiro, L.A.**, **Jimenez-Espejo, F.J.**, **Bahr, A.**, **Flores, J.A.**, **Ausin, B.**, **Rogerson, M.**, **Lozano-Luz, R.**, **Lebreiro, S.M.** and **Hernandez-Molina, F.J.** (2020) Mediterranean overflow over the last 250 kyr: freshwater forcing from the tropics to the ice sheets. *Paleoceanogr. Paleocl.*, **35**. https://doi.org/10.1029/2020pa003931

Simon, D., **Marzocchi, A.**, **Flecker, R.**, **Lunt, D.J.**, **Hilgen, F.J.** and **Meijer, P.T.** (2017) Quantifying the Mediterranean freshwater budget throughout the late Miocene: new implications for sapropel formation and the Messinian Salinity Crisis. *Earth Planet Sci. Lett.*, **472**, 25–37.

Simon, D. and **Meijer, P.T.** (2017) Salinity stratification of the Mediterranean Sea during the Messinian crisis: A first model analysis. *Earth Planet. Sci. Lett.*, **479**, 366–376.

Spakman, W., **Chertova, M.V.**, **van den Berg, A.** and **van Hinsbergen, D.J.** (2018) Puzzling features of western Mediterranean tectonics explained by slab dragging. *Nat. Geosci.*, **11**, 211–216.

Stow, D.A.V. (1985) Fine-grained sediments in deep water: An overview of processes and facies models. *Geo-Mar. Lett.*, **5**, 17–23.

Stow, D.A.V. and **Faugères, J.C.** (2008) Contourite facies and the facies model. *Dev. Sedimentol.*, **60**, 223–256.

Stow, D.A.V., **Hernández-Molina, F.J.**, **Llave, E.**, **Sayago-Gil, M.**, **Díaz del Río, V.** and **Branson, A.** (2009) Bedform-velocity matrix: the estimation of bottom current velocity from bedform observations. *Geology*, **37**, 327–330.

Stow, D.A.V., **Hernández-Molina, F.J.**, **Llave, E.**, **Bruno, M.**, **García, M.**, **del Rio, V.D.**, **Somoza, L.** and **Brackenridge, R.E.** (2013) The Cadiz Contourite Channel: Sandy contourites, bedforms and dynamic current interaction. *Mar. Geol.*, **343**, 99–114.

Stow, D.A.V. and **Piper, D.J.W.** (1984) Deep-water fine-grained sediments: facies models. *Geol. Soc. London. Spec. Publ.*, **15**, 611–646.

Stow, D.A.V. and **Smillie, Z.** (2020) Distinguishing between deep-water sediment facies: Turbidites, contourites and hemipelagites. *Geoscience*, **10**, 68.

Stow, D.A.V. and **Wetzel, A.** (1990) Hemiturbidite: a new type of deep-water sediment. In: *Proceedings of the Ocean Drilling Program, Scientific Results* (Eds Cochran, J.R. and Stow, D.A.V.), pp. 25–34. Ocean Drilling Program, College Station, TX. Available at: http://www-odp.tamu.edu/publications/116_sr/volume/chapters/sr116_03.pdf

Straume, E.O., **Gaina, C.**, **Medvedev, S.** and **Nisancioglu, K.H.** (2020) Global Cenozoic Paleobathymetry with a focus on the Northern Hemisphere Oceanic Gateways. *Gondwana Res.*, **86**, 126–143.

Talling, P.J., **Masson, D.G.**, **Sumner, E.J.** and **Malgesini, G.** (2012) Subaqueous sediment density flows: Depositional processes and deposit types. *Sedimentology*, **59**, 1937–2003.

Taltasse, P. (1953) Recherches géologiques et hydrogéologiques dans le Bassin lacustre de Fès-Moknès. *Notes & M. Serv. géol. Maroc.*, 78–81.

Tulbure, M.A., **Capella, W.**, **Barhoun, N.**, **Flores, J.A.**, **Hilgen, F.J.**, **Krijgsman, W.**, **Kouwenhoven, F.J.**, **Sierro, F.J.** and **Yousfi, M.Z.** (2017) Age refinement and basin evolution of the North Rifian Corridor (Morocco): No evidence for a marine connection during the Messinian Salinity Crisis. *Palaeogeogr. Palaeoclimatol. Palaeoecol.*, **485**, 416–432.

Uchman, A. (2009) The Ophiomorpha rudis ichnosubfacies of the Nereites ichnofacies: characteristics and constraints. *Palaeogeogr. Palaeoclimatol. Palaeoecol.*, **276**, 107–119.

Van Assen, E., **Kuiper, K.F.**, **Barhoun, N.**, **Krijgsman, W.** and **Sierro, F.J.** (2006) Messinian astrochronology of the Melilla Basin: stepwise restriction of the Mediterranean-Atlantic connection through Morocco. *Palaeogeogr. Palaeoclimatol. Palaeoecol.*, **238**, 15–31.

Vázquez, A., **Bruno, M.**, **Izquierdo, A.**, **Macías, D.** and **Ruiz-Cañavate, A.** (2008) Meteorologically forced subinertial flows and internal wave generation at the main sill of the

Strait of Gibraltar, Deep-Sea Research Part I. *Oceanogr. Res. Pap.*, **55**, 1277–1283.

Viana, A.R., **Faugères, J.C.** and **Stow, D.A.V.** (1998) Bottom-current-controlled sand deposits—a review of modern shallow-to deep-water environments. *Sediment. Geol.*, **115**, 53–80.

Visser, M.J. (1980) Neap-spring cycles reflected in Holocene subtidal large-scale bedform deposits: a preliminary note. *Geology*, **8**, 543–546.

de Weger, W., **Hernández-Molina, F.J.**, **Flecker, R.**, **Sierro, F.J.**, **Chiarella, D.**, **Krijgsman, W.** and **Manar, M.A.** (2020) Late Miocene contourite channel system reveals intermittent overflow behavior. *Geology*, **48**, 1194–1199.

Wernli, R. (1988) Micropaléontologie du Néogène post-nappes du Maroc septentrional et description systématique des foraminifères planctoniques. *Notes et Mémoires du Service géologique*, **331**, 270. Available at: https://pascal-francis.inist.fr/vibad/index.php?action=getRecordDetail&idt=19259060

Manuscript received 8 October 2020; revision 25 March 2021; revision accepted 5 April 2021

Supporting Information

Additional information may be found in the online version of this article:

Fig. S1. Microphotographs for facies F4 and F5.
Fig. S2. Microphotographs for facies F6 and F8.
Table S1. Modal analysis data based on 300-point counts in thin section.